Similarities in Meteorological Composites Among Different Atmospheric River Detection Tools During Atmospheric River Landfall.

Kwesi Twentwewa Quagraine[1], Travis Allen O'Brien[1], and Mohammad Rubaiat Islam[1]

[1]Indiana University Bloomington

April 16, 2024

Abstract

Many atmospheric river detectors (ARDTs) have been developed over the past few decades to capture atmospheric rivers (ARs). However, different ARDTs have been observed to capture different frequencies, shapes and sizes of ARs. Due to this, many questions including investigating the underlying phenomena for ARs in the ARDTs have been posed. In this paper, we assess four different ARDTs and investigate the underlying meteorological phenomena during landfalling ARs. We find that during landfalling ARs events, there exists a prevalent low-pressure and high-pressure confluence that enhances moisture influx toward the landfalling site. The strength of the pressure gradient in the confluence region enhances the influx of the integrated vapor transport. The four ARDTs predominantly capture similar atmospheric processes, nonetheless, they have statistically different magnitudes.

Similarities in Meteorological Composites Among Different Atmospheric River Detection Tools During Atmospheric River Landfall.

Kwesi T. Quagraine [1], Travis A. O'Brien [1,2], Mohammad Rubaiat Islam [1]

[1]Earth and Atmospheric Science Department, Indiana University Bloomington, USA
[2]Climate and Ecosystem Sciences Division, Lawrence Berkeley National Laboratory, Berkeley, CA, USA

Key Points:

- The four ARDTs assessed predominantly capture similar atmospheric processes, however, with statistically significant difference in magnitudes.
- Landfalling ARs have a prevalent low-pressure and high-pressure confluence that enhance moisture influx toward the AR landfalling site.
- During consensus times, IVTs are higher as compared to non-consensus times.

Corresponding author: Travis A. O'Brien, `obrienta@iu.edu`

Abstract

Many atmospheric river detectors (ARDTs) have been developed over the past few decades to capture atmospheric rivers (ARs). However, different ARDTs have been observed to capture different frequencies, shapes and sizes of ARs. Due to this, many questions including investigating the underlying phenomena for ARs in the ARDTs have been posed. In this paper, we assess four different ARDTs and investigate the underlying meteorological phenomena during landfalling ARs. We find that during landfalling ARs events, there exists a prevalent low-pressure and high-pressure confluence that enhances moisture influx toward the landfalling site. The strength of the pressure gradient in the confluence region enhances the influx of the integrated vapor transport. The four ARDTs predominantly capture similar atmospheric processes, nonetheless, they have statistically different magnitudes.

Plain Language Summary

Atmospheric rivers (ARs) are an atmospheric phenomena that is responsible for transporting water vapor from the warm tropics to the cold polar regions. As they transport, they rain out the transported water vapor. Due to their influence on precipitation, researchers have developed different methods in tracking them. In an attempt to track them, it is observed that the different AR identification methods capture different frequencies and sizes during AR propagation and landfall. These differences have raised questions concerning the prevailing meteorological phenomena during ARs. In this paper, we assess four ARDTs during landfalling AR events and investigate their prevailing meteorological phenomena. We find that all four ARDTs predominantly capture similar meteorological phenomena, however, with statistically different magnitudes.

1 Introduction

Atmospheric rivers (ARs) are a type of weather phenomenon that is important for moving water from the warm, moist tropics to the cool dry polar regions (Zhu & Newell, 1998; Guan et al., 2010; M. Dettinger, 2011; F. M. Ralph & Dettinger, 2011; O'Brien et al., 2020). ARs are associated with storm tracks and result in extreme winds, and substantial amounts of precipitation which result in floods and large snow packs (M. D. Dettinger, 2013; M. Dettinger, 2011; Neiman et al., 2008; F. M. Ralph & Dettinger, 2011; Payne & Magnusdottir, 2014; Guan et al., 2010). The literature shows that about 40% of high precipitation events on the west Indian coast (Dhana Laskhmi & Satyanarayana, 2020) and $\sim$70% of heavy precipitation events over South Africa (Blamey et al., 2018) are associated with ARs. Over the Western U.S. and other water-stressed areas, weak ARs produce beneficial rain and snow that is an important source of freshwater (Guan et al., 2010; M. Dettinger, 2011; Rutz & Steenburgh, 2012; Kunkel & Champion, 2019) and may be a relief for drought conditions in some regions (M. D. Dettinger, 2013). Over the west coast of North America, studies have shown that ARs contribute to precipitation as much as 15 to 35% over southern California and about 25 to 60% over coastal Washington (M. Dettinger, 2011; Rutz et al., 2014; Guan & Waliser, 2015). In summary, ARs contribute about 50% of the total annual precipitation over North America (Gershunov et al., 2019). Although these AR-induced precipitations sometimes alleviate water stress over the region, some of these precipitation events have led to extreme precipitation events. (Lamjiri et al., 2017; Barth et al., 2017). In the western United States of America (USA), it is projected that the number of AR-induced extreme precipitation events may increase whereas the overall frequency of non-AR-related precipitation may decrease (Lavers & Villarini, 2015; Williams et al., 2020). Although all other AR-prone regions in the world are not spared of these AR-induced extreme events, this work focuses on AR events in the northern Pacific basin due to the well-documented impacts once they make landfall over the region (Payne & Magnusdottir, 2014; F. M. Ralph et al., 2019).

Although the literature shows a clear association between ARs and extreme precipitation events (Barth et al., 2017; F. M. Ralph et al., 2019), recent studies have started associating ARs with extreme heat events. Such events include the summer heat wave event over the northwestern coast of North America in 2021 (Mo et al., 2022). In this event, there were record-breaking temperatures of about 46 ^{o}C. This resulted in heat strokes and other heat-related diseases in the region (Mo et al., 2022). Also, an extreme high-temperature event recorded over coastal East Antarctica in 1989 has recently been attributed to AR influx into the region (Turner et al., 2022). Turner et al. (2022) show in their findings that "Sustained horizontal warm advection toward the coast of East Antarctic via an atmospheric river led to the marked warming".

The effects associated with ARs have led to a large amount of research on AR frequency, intensity, variability, and change (M. Dettinger, 2011; Mundhenk et al., 2016; Lavers & Villarini, 2015); others have investigated AR morphology and other aspects of AR evolution including size, water content, windiness, et cetera (Payne & Magnusdottir, 2015, 2016; Doiteau et al., 2021). Other research has investigated the correlations between signatures of ARs and climate model indices (like El- Niño Southern Oscillation (ENSO) and Madden-Julian Oscillation(MJO)) and observed that ENSO modulates the latitude of landfalling ARs. Also, most landfalling AR dates occur during El Niño. The MJO is shown to modulate the intensity of landfalling ARs, as well as precipitation totals(Payne & Magnusdottir, 2014). Payne and Magnusdottir (2014); Neiman et al. (2008) have also investigated AR dynamics and have shown that during ARs there is a synoptic scale low pressure on the northwestern side and a high pressure on the southeastern side of the region of intense IVT characterized as the AR. Also, ARs have been associated with frontal boundaries; both oceanic and atmospheric fronts (Xiong & Ren, 2021; Neiman et al., 2008). Other research suggests that some ARs form in association with the warm conveyor belt of extratropical cyclones and they may not necessarily be associated with just one cyclone but can span the lifetimes of multiple cyclones (Payne & Magnusdottir, 2014). Ryoo et al. (2013) found that moisture transport in ARs is somewhat modulated by the subtropical jet and also the location of the Rossby wave breaking along the west coast of North America. In an attempt to understand AR morphology, Payne and Magnusdottir (2014) have also shown that ARs have an association with Rossby waves. Their findings also conclude that ARs are modulated by the influence of the tropical on the extratropical but their variability is more strongly tied to extratropical dynamics than tropical dynamics. The co-occurrence of ARs with other phenomena such as Pacific Decadal Oscillation (PDO) (Gershunov et al., 2017) and Arctic Multidecadal Oscillations (AMO) (Zhang et al., 2021) have been investigated in the literature. One understudied phase of these experiments to understand ARs is that most of the various planetary scale phenomena research was conducted using one ARDT, therefore suggesting that we should consider an ensemble of ARDTs to investigate if these findings are true for all ARDTs.

Studies over the years have looked at different methods to categorize, track, and count the number of ARs in the atmosphere at any given time (O'Brien et al., 2020; Inda-Díaz et al., 2021; Guan & Waliser, 2015; Lavers et al., 2012). From region to region, the availability of water vapor, wind speeds and direction, geopotential height, jet stream location and phase speeds, vertical profile, and many other meteorological variables may play a substantial role in the genesis, evolution, transport, landfall, and breaking of the AR (F. Ralph et al., 2013; F. M. Ralph et al., 2004; Bao et al., 2006; Jankov et al., 2009; Guan & Waliser, 2015). Scientists have developed different metrics or algorithms for characterizing ARs using these meteorological variables. Basically, most atmospheric river detectors (ARDTs) are a set of algorithms that set a threshold on the spatial extent and water vapor transport in the troposphere and call them atmospheric river objects. Due to the vast number of ARDTs being developed, the Atmospheric Rivers Tracking Method Intercomparison Project was started with the aim of collating and investigating the experimental designs of various AR algorithms (Rutz et al., 2019a).

Since the inception of ARTMIP, many ARDTs have been collated and implemented on a specific common dataset for a defined period of time. The ARTMIP project comprises two phases (i.e, Tier 1 which uses the Modern Era Retrospective-analysis for Research and Applications (MERRA - 2) as a baseline for comparisons, and Tier 2 which includes sensitivity studies designed around specific scientific questions (C. A. Shields et al., 2018; O'Brien et al., 2020). Although all these ARDTs use similar datasets, they have different levels of "permissiveness" as to what should be characterized as an AR. This permissiveness leads to differences in their AR frequencies, intensities, duration, and attribution of high-impact weather and climate events to ARs (C. A. Shields et al., 2018; Lora et al., 2020).

More often than not, AR detection studies use either the integrated water vapor (IWV) like Goldenson et al. (2018); Hagos et al. (2015); Kashinath et al. (2021) or the integrated vapor transport (IVT) like Leung and Qian (2009); Lora et al. (2017); Mahoney et al. (2016) and many others. These variables (IVT and IWV) over the years have been assessed to know which of them gives a better characteristic for AR detection and attribution. Junker et al. (2008) and F. Ralph et al. (2013) in their work show that IVT is more strongly correlated with cool season precipitation as compared to IWV. IVT also penetrates further inland and is spatially co-located with regions of precipitation more than IWV. Due to the difference in variable preference and thresholding values for these variables (i.e., IVT and IWV), ARDTs capture different frequencies, intensities, and structures of ARs. Therefore some researchers clearly state their preference to use IVT as opposed to IWV (Nayak et al., 2014; Rutz et al., 2014).

Aside from the disparities in IVT or IWV selection and preference based on specific scenarios, the basic idea for AR detection is the use of IVT or IWV thresholds. Some studies either use an absolute categorization method – a specific threshold is set for all instances – or a relative categorization method – the threshold changes based on an event. Other ARDTs also use tracking algorithms. In these tracking algorithms, a Lagrangian-style detection is used, where ARs are considered as objects being tracked. For instance Lavers et al. (2012) use the median IWV percentile as the threshold for categorizing ARs over western Europe, Kashinath et al. (2021) use machine learning based on segmentation, trained on 500 expert labeled images to track AR associated extreme events. Lora et al. (2017) use Integrated Vapor Transport that is 100 $kgm^{-1}s^{-1}$ above climatological area means for North Pacific as a criterion for categorizing ARs. These and many other ways have been used to categorize ARs in literature. Although IVT and IWV are the main components of detecting ARs, there are other atmospheric parameters that are sometimes coupled with these two due to their supposed influence on the detection algorithms. In Lora et al. (2017) winds and precipitation are included in their detection of ARs. Many of these differences in literature lead to the question: Do all ARDTs observe similar weather phenomena when they detect ARs?

The methods for detecting ARs have proved to be fundamentally consistent with each other on what we "normally" classify as an AR (C. A. Shields et al., 2023), however, ARDTs capture these AR objects in different frequencies, intensities, shapes, and sizes (Inda-Díaz et al., 2021; C. A. Shields et al., 2018; Rutz et al., 2019b). In this work, we investigate the underlying meteorological phenomena that govern a specific set of ARDTs and hypothesis that different ARDTs capture different meteorological phenomena during AR landfall. This hypothesis stems from evidence that different ARDTs capture different frequencies (C. A. Shields et al., 2018) of ARs and, as such, may have different weather conditions during AR detection for any given ARDT. Also, the intensity of these captured ARs would depend on the weather preceding the AR. Therefore, this work seeks to characterize the meteorological phenomena associated with four commonly used ARDTs and investigate the meteorological phenomena associated with the intensity and frequency of the occurrence of the ARs in the specific ARDT over the west coast of the United States.

2 Method

In this work we attempt to identify different weather phenomena that are associated with different ARDTs. In so doing, we use specific AR-related variables like potential vorticity, total column of water vapor, IVT, geopotential heights, temperature, and mean sea level pressure. These variables are selected due to their suggested influence on moisture transport and general atmospheric circulation (T.-J. Zhou & Yu, 2005; Bao et al., 2006; Kim et al., 2019). We focus on the December-February (DJF) period. Climatologically, over the west coast of the US, the impacts of ARs that make landfall along the area are mostly within this period (Neiman et al., 2008; Payne & Magnusdottir, 2014; F. Ralph et al., 2013; Mundhenk et al., 2016).

2.0.1 Consensus Times (CT) and Non-consensus Times (NCT)

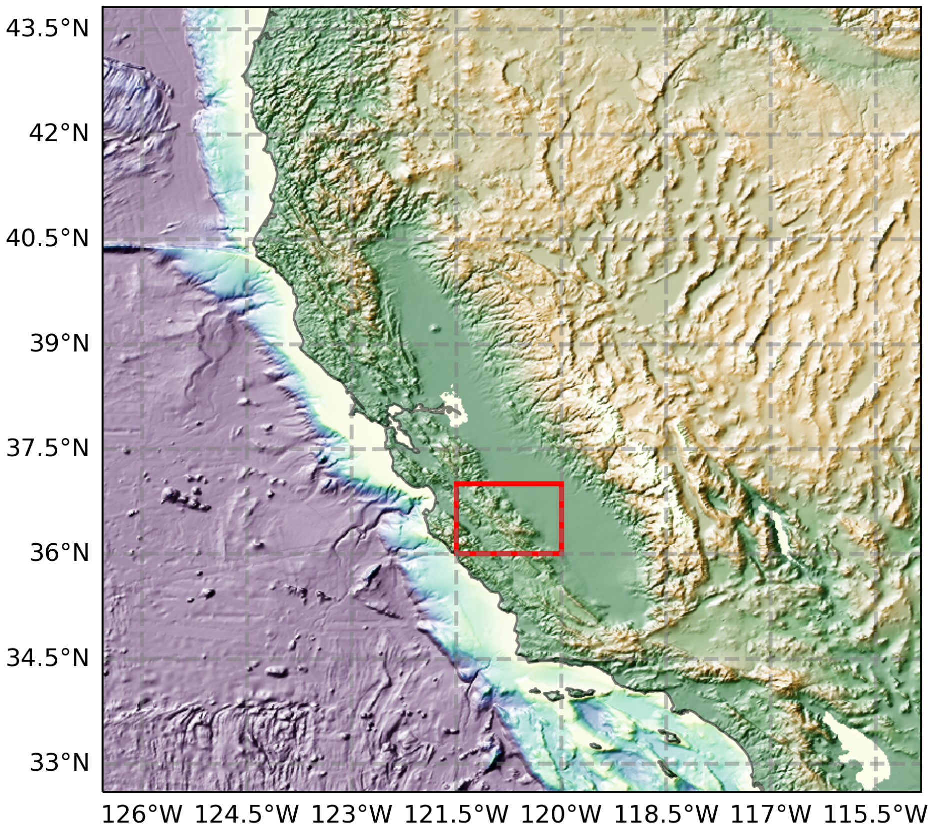

Figure 1. Map of the west coast of the United States of America. The red box represents the landfalling AR region selected to show consensus.

To independently select land falling ARs that are representative of the various algorithms, a region which is well impacted by ARs (M. Dettinger, 2011; Neiman et al., 2008), is selected along the west coast of the Continental United States (CONUS), and the frequency of landfalling ARs over the region (red box in Figure 1) are captured. Consensus times (CT), which are times where all ARDTs captured ARs are grouped apart from non-consensus times (NCT). By definition, these consensus times have the same phenomena for all algorithms under study since the meteorology at those timesteps is from the same datasets. NCTs are days that do not coincide in all four ARDTs. This means there is a probability of some days being alike in 2 or 3 algorithms however, they are not recognized as CT days because they do not meet the criteria of consensus (that is, all 4 algorithms must capture that time).

2.0.2 Anomaly

Anomalies (deviations from the climatology) are computed for the NCT ARs using the climatologies from the DJF season since the focus of ARs in this study is in that season. To compute the climatology, the DJF season (winter) for the entire temporal regime is selected and the mean is computed using this sample. Spatial anomalies show the magnitude of change of a variable from its climatology at a data point. This is computed as

$$\bar{V} = \frac{1}{M}\sum_{i}^{J} X_i \qquad \{where\ X_i \in NCTs\ or\ CTs\} \tag{1}$$

$$\bar{V}^y = \frac{1}{N}\sum_{i}^{J} Y_j \qquad \{where\ Y_j \in DJF\ in\ every\ year\} \tag{2}$$

$$V_{anom} = \bar{V} - \bar{V}^y \tag{3}$$

where $\bar{V}$ is the average CT or NCTs captured in an ARDT and $\bar{V}^y$ is the climatological mean of DJFs every year.

2.0.3 Bootstrapping

To test the significance of the anomaly, bootstrapping is used to test the null hypothesis that all ARDTs capture ARs under the same meteorological phenomena and magnitude. If the null hypothesis is false, then differences in meteorological composites between two ARDTs should be statistically different from zero. We use a bootstrapping procedure, described in the next paragraph, to estimate the distribution of differences between NCT composites for each grid cell.

To formulate this bootstrapping test, we do the following. We randomly sample with replacement all timesteps in the datasets and compute the mean over time for every bootstrap sample. We repeat this random sampling process for 1000 bootstrap samples. These samples are concatenated into one dataset. The bias between the bootstrap ($\Delta = X_1^b - X_2^b$, where X_1^b and X_2^b represents bootstrapped datasets and Δ is the difference between 2 datasets) samples for the algorithms is computed. This bias, if centered around 0 shows that the results between 2 specific algorithms are not statistically different for a specific atmospheric variable. However, if the bias between the samples is different from 0, then we use the student's t-test as the test for significance. This process is repeated for all variables and all gridcells to check the statistical significance of the phenomena being observed.

3 Data

We mostly use the ARTMIP database for obtaining the various ARDTs. In this catalog, AR detection algorithms were run using the same dataset for the derived variables, IWV and IVT from Modern-Era Retrospective Analysis for Research and Applications

(MERRA-2)(Gelaro et al., 2017). We consider the Tier 1 ARTMIP data catalog from 1980 to 2017 (C. A. Shields et al., 2018). Prior to ARTMIP, most AR algorithms used different datasets and were for specific regions, however, in ARTMIP Tier 1, the same datasets were used and also some algorithms were run for the entire globe (C. A. Shields et al., 2018). The ARTMIP catalog contains ARDTs computed on 3-hourly timescales and each grid point is tagged using binary indicators (0 for no AR presence and 1 for AR presence) (C. A. Shields et al., 2018). The catalog for the datasets can be found in C. Shields (2019).

Here, we focus mainly on 4 algorithms submitted to the ARTMIP Tier 1, that is, the Guan & Waliser (Guan & Waliser, 2015), Mundhenk v2 (Mundhenk et al., 2016), TECA BARD v1 (O'Brien et al., 2020) and the Reid250 (Reid et al., 2020) algorithms. These specific algorithms were chosen because they are all computed using the same variable (i.e., IVT, which inculcates the direction of flow in its calculation unlike the IWV which is the amount of water vapor in the atmosphere at a specific time) and most importantly, they cover the 3 major categories of ARDTs previously discussed: relative, absolute, and percentile-time detection.

To account for the meteorology associated with ARDTs, we consider the European Centre for Medium-Range Weather Forecast's (ECMWF) Reanalysis 5 (ERA5) dataset. We select a few of the variables which include the total column of water vapor (TCWV), IVT, mean sea level pressure (MSL), potential vorticity at 500 hPa (PV), geopotential heights at 500 hPa (GEOPTH) and 500 hPa temperature. These variables are selected based on their ability to detect most synoptic scale features that are associated with precipitable water, its transport, and the meteorology that occur during their existence (T.-J. Zhou & Yu, 2005; Bao et al., 2006; Kim et al., 2019). These quantities have proven to be representative of mid-latitude dynamics and are generally used in mid-latitude studies and textbooks (Bluestein, 1992; McIntyre, 2003). Also, past research hints at their importance for mid-latitudinal atmospheric transport (McIntyre, 2003). The ERA5 dataset has a spatial resolution of $0.25^o \times 0.25^o$ and a temporal resolution of 1 hour with 37 levels for atmospheric variables with levels. The entire duration of data considered in this study is from 1979 to 2017 (Hersbach et al., 2020).

4 Results

The results show that there are differences between ARDTs during CTs and NCTs (Table 1). Table 1 shows that TECA_BARD v1 (Guan & Waliser) is the most restrictive (permissive) ARDT among the four. TECA_BARD v1 (Guan & Waliser) has the least (highest) fraction of AR counts particular to it. These differences in frequencies are consistent with C. A. Shields et al. (2018) which reflects that there are differences in AR frequencies across ARDTs. Unique times where ARs are captured separately from any other ARDT show that TECA_BARD is the ARDT in the least disagreement with all other ARDTs on what describes an AR. Guan & Waliser is the algorithm with the highest disagreement as compared to other ARDTs. The spatial distribution of these frequencies can be seen in supplemental figures (SA1 and SA2).

We investigate some atmospheric variables to observe the spatial orientation of meteorology associated with the CTs of ARs. For CTs, Figures 2 (a) and (b) shows that in CTs there are large positive IVT anomalies ($\sim > 300$ kgm^{-2}s^{-2}), positive TCWV anomalies with the highest of ~ 10 kgm^{-2}, and generally warm 500 hP temperature anomalies ($\sim$ 4K) anomalies along the landfall region. This orientation of column variables is coupled with a low-pressure anomaly along the Aleutian low and a 500 hPa trough in the geopotential height. The atmospheric orientation shows a strong temperature gradient which has its low superimposed on the low-pressure anomaly over the Pacific Northwest (PNW) and the high-temperature anomaly over land.

	TECA_BARD v1	Guan & Waliser	Mundhenk v3	Reid 250
Consensus times (CTs)	279 (42.86%)	279 (9.95%)	279 (21.54%)	279 (21.68%)
Non-consensus times (NCTs)	379 (57.14%)	2526 (90.05%)	1016 (78.46%)	1008 (78.32%)
Total number of ARs	658	2805	1295	1287
Unique ARs	9 (1.38%)	1170 (41.71%)	34 (2.63 %)	88 (6.84%)

Table 1. Table showing the algorithms and the number of consensuses, Non-consensus, and unique ARs and their percentages with respect to the total number of ARs captured in an ARDT. Text in red represents the most restrictive (Consensus times) and most permissive (Non-consensus times).

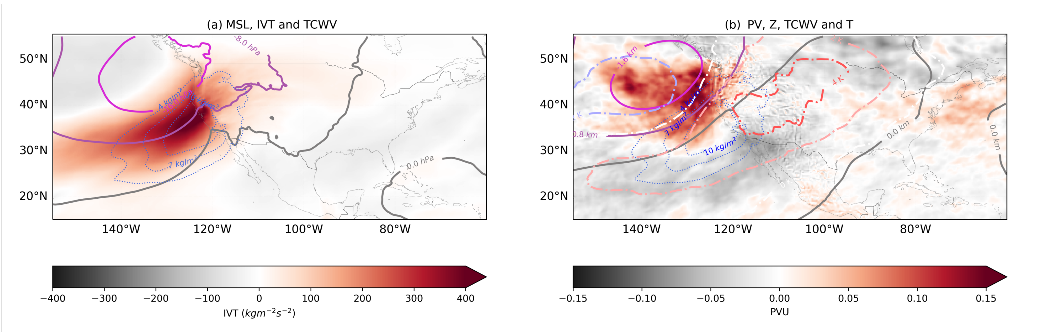

Figure 2. DJF Consensus times composites for atmospheric variables; IVT (grey, white, and red shading), MSL (magenta, grey, and dark red solid line), TCWV (blue dots) panel (a) and 500 hPa Potential Vorticity (grey, white, and red shading) 500 hPa temperature (blue white red dashed dot line) and 500 hP geopotential heights (magenta, grey, brown solid line) (b) [Red square represents the AR region]

Comparatively, the anomalies in the NCTs (Figure 4 and 3) are of smaller magnitudes as compared to the CTs (Figure 2). This suggests that all ARDTs are able to capture AR frequencies that have pronounced atmospheric conditions. In other words, the more extreme an AR is, the higher the possibility that an ARDT may capture it.

The ARDTs show different orientations of IVT along the landfall region (Figure 3). Unlike all other ARDTs, TECA_BARD v1 shows a more westerly flow of moisture. All ARDTs except TECA_BARD v1 have a cut-off of IVT anomaly right around the 0 hPa surface pressure anomaly. TECA_BARD v1 ARDT tends to capture more IVT within the AR column as compared to the other ARDTs. Over the 500 hPa level (Figure 4), the Guan & Waliser ARDT shows a cooler mid-column of IVT. The Reid 250 ARDT has the warmest mid-tropospheric column of ARs. Although the mid-troposphere for Reid 250 is warm, the highest warmth ($\sim$ 4K) is located about 5^o east from the landfalling region and also further dissociated from the column of high IVT anomaly. TECA_BARD however has the most elongated column of positive temperature anomaly. This is consistent with the results from Mo et al. (2022) who suggest that ARs are associated with tropospheric heating. TECA_BARD v1 is observed to have an entirely warm column of IVT over the landfall region and over the region of intense IVT anomaly (the AR column). The result from

TECA_BARD v1 compares well with CT's atmospheric patterns. This warm layer in TECA_BARD v1 is accompanied by positive 500 hPa height anomalies that are not observed in any of the ARDTs. The surface low-pressure anomaly (Figure 3) located on the Northwest of the landfall region for all ARDTs shows a corresponding upper-level (500 hPa) negative geopotential anomaly (Figure 4) in all ARDT.

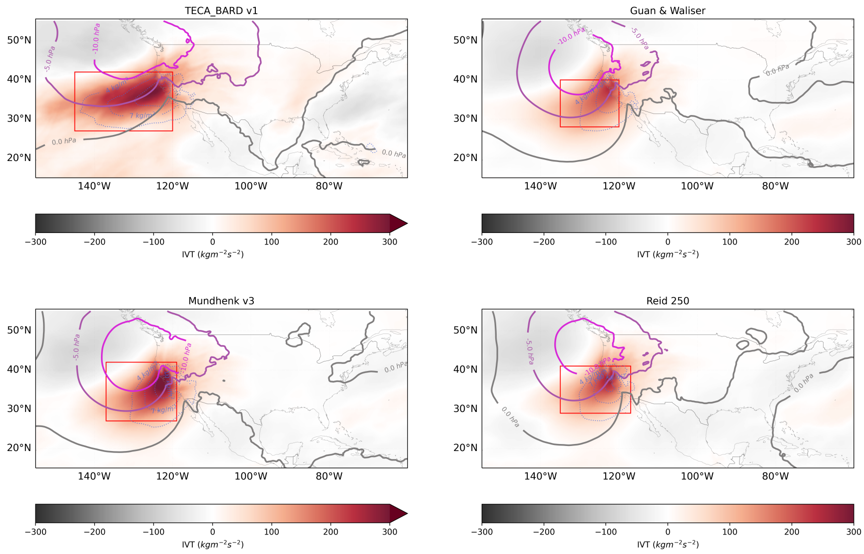

Figure 3. DJF Non-consensus times composites for atmospheric variables; IVT (grey, white, and red shading), MSL (magenta, grey, and dark red solid line), TCWV (blue dots) [Red square represents the AR region]

Over the landfalling region, we assess the difference in magnitudes of composites in Figure 5. Values of IVT and TCWV for TECA_BARD v1 are higher at the landfall site as compared to all other ARDTs, hence, the positive displacement of the PDF for any ARDT and TECA_BARD v1 difference. PV differences show that for all ARDTs, there is substantial instability which is observed in the positive PV anomalies. This implies there is expansion in the air column (warmth) and potential for rotation along the landfall region. TECA_BARD v1 tends to have the highest instability and rotation in the PV field. At the 500 hPa heights (Z plots), TECA_BARD v1 which has the warmest area within the landfall region also has the highest heights when compared with all other ARDTs.

The differences in the various magnitudes of composites for the ARDTs suggest that the differences are statistically significant for each ARDT. Figure 6 shows the significance plot for IVT between the ARDTs as the shading and the significance at 90%, 95%, and 99% levels. Over AR and landfalling region, there are statistically significant differences between all ARDTs. These differences are more pronounced in the MSL confluence region for all ARDTs. For all other variables assessed here, ARDTs show a statistically significant difference. This suggests although ARDTs may show similar spatial orientations (with slightly different spatial extents) of atmospheric phenomena during ARs, the magnitudes of atmospheric conditions for all ARDTs are statistically significantly dif-

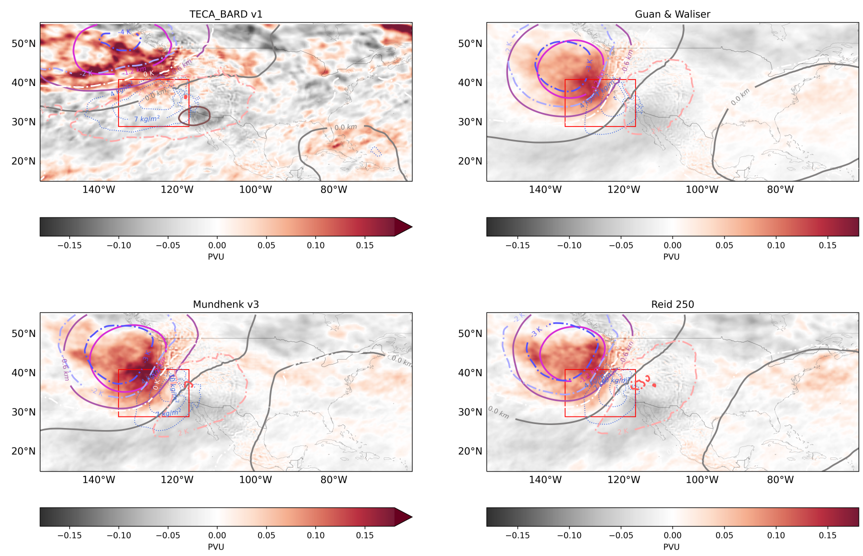

Figure 4. DJF Non-consensus times composites for atmospheric variables; Potential Vorticity (grey, white, and red shading) 500 hP temperature (blue white red dashed dot line) and 500 hP geopotential heights (magenta, grey, brown solid line) [Red square represents the AR region]

ferent from each other (see also supplementary figures). However, the difference in PV anomalies for ARDTs did not show any statistical significance for all ARDTs.

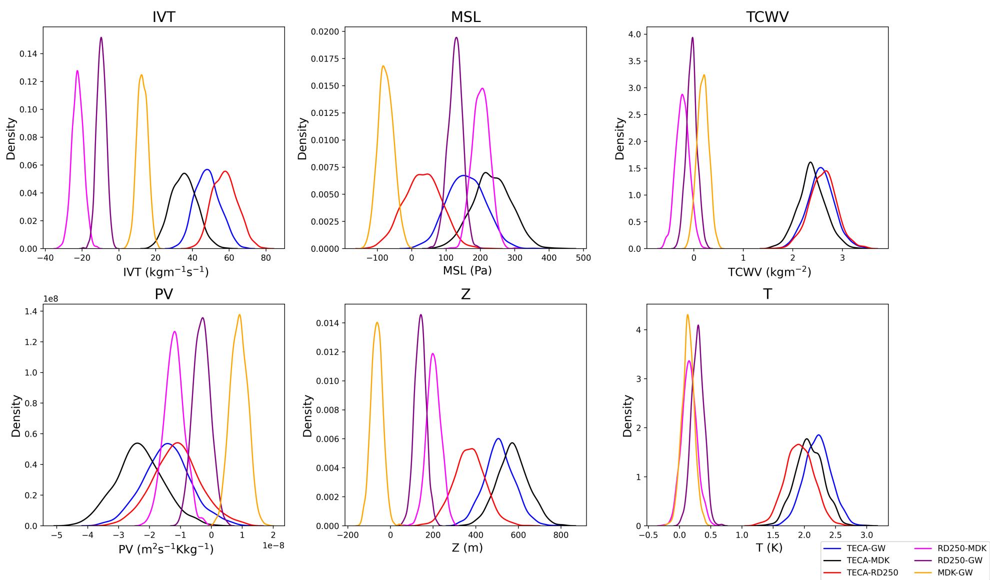

Figure 5. Probability distribution of differences in atmospheric variables for the various ARDTs between 145^{o}W to 118^{o}W and 25^{o}N to 45^{o}N

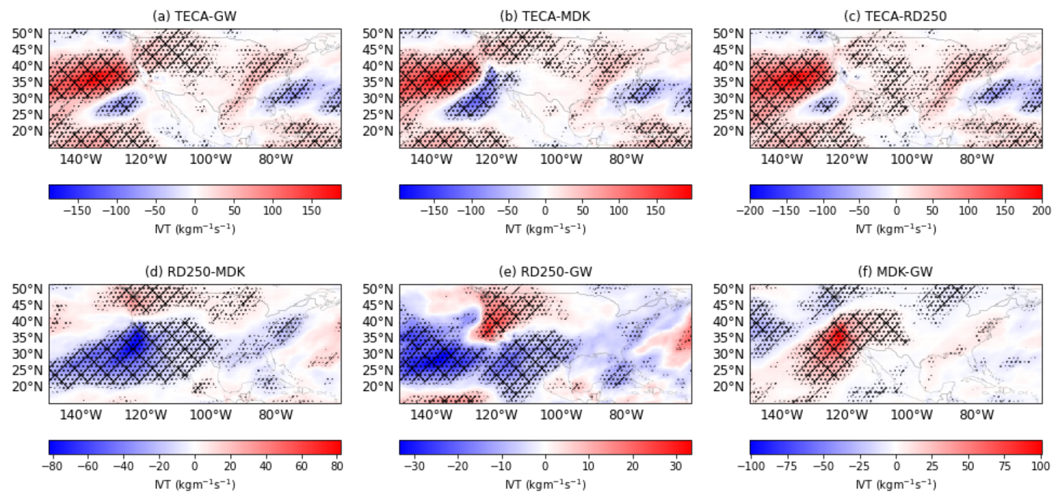

Figure 6. IVT difference plots between ARDTs (shading). Significance computed at 99% (/), 95% (//), and 90%(..) confidence intervals using the student t-test.

5 Summary and Discussion

ARs are proving to be more influential in mid-latitude weather than previously understood. Previous research (i.e., about 2 decades ago) has looked at the influence of precipitation caused by ARs, however, over the last decade, research has shown that ARs are not merely associated with precipitation, but also extreme precipitation and some heat waves (Liu et al., 2021; O'Brien et al., 2022; Mo et al., 2022). One may argue that these effects may not be well represented in all ARDTs, which may be true due to the preference for detection. For permissive ARDTs, these signals of extreme precipitation may be reduced in composite precipitation data as opposed to restrictive ARDTs. Here, we have looked at using different ARDTs which have different levels of permissiveness to assess the meteorology behind ARs during landfall. Using single ARDTs could be beneficial for specific regions based on the method of AR categorization. For instance, Guan & Waliser would be good for studies along tropical regions because it is not latitudinally filtered (Guan & Waliser, 2015), whereas TECA_BARD v1 may not be a good choice for tropical regions because of its Gaussian latitudinal filter (O'Brien et al., 2020) used to dampen the Inter Tropical Convergence Zone (ITCZ) and as a result, captures stronger ARs as seen in Figure 3, the use of the Mundhenk algorithm may be beneficial for characterizing ARs specific to time and location since they use a time and spatially varying percentile categorization (Mundhenk et al., 2016), the Pan and Lu (2019) algorithm uses both a local and global filter to make the capture of ARs in the polar regions more characteristic of the region due to lower water vapor presence in the region as opposed to other parts of the globe where there is substantial water vapor. These different algorithm structures and detection mechanisms show the potential difference in frequency, intensity, and duration of ARs. So in our work, we use these different ARDTs over a region where they all capture ARs and assess the meteorology. The results from composites obtained are generally in agreement which suggests that these ARDTs might be capturing the same meteorological phenomenon (apparently a midlatitude cyclone) at different phases of its evolution. With these findings, we refuse to accept the hypothesis that ARDTs capture different meteorological phenomena during landfall over the western coast of CONUS using different ARDTs.

ARDTs have proved to detect different flavors of ARs (Gonzales et al., 2020; Y. Zhou et al., 2022). These flavors are mostly a result of what ARDTs classify as ARs. As such we have assessed composites for landfalling ARs and their surrounding meteorological phenomena focusing on the DJF season. Four ARDTs are assessed; TECA_BARD v1, Guan & Waliser, Reid 250 and Mundhenk v3. These ARDTs capture different AR frequencies (counts) over a landfall region. From the number of counts, we are able to determine that for specific times, all four ARDTs agree on the presence of an AR in the vicinity of landfall (CTs). However, the majority of ARs detected by these ARDTs are mostly not in consensus (NCTs). We further assess unique times when only an ARDT captures an AR apart from the other ARDTs. Results show that TECA_BARD v1, Reid 250, and Mundhenk v3 ARDTs are mostly in agreement with either one of the four ARDTs, however, Guan & Waliser ARDT tends to not be in agreement as much (Table 1). The Mundhenk and Reid250 ARDTs show similar results as the Guan & Waliser ARDT with a reduction in the frequency and shape of landfalling ARs. Aside from the difference in the number of ARs and their respective times of capture, it is observed that there are different angles subtended by ARs in the ARDTs (see also Figure A1 and A2). These different spatial orientations can be observed directly from the orientations in composites. For instance, the region of steepest gradient between the high-pressure and the low-pressure systems generally determines the location of the AR. This is consistent Guirguis et al. (2019)'s findings that different surface orientations may influence the location and orientation of an AR.

In general, there is an agreement between all ARDTs on the prevailing meteorological phenomena during AR landfall, however, the magnitudes and orientations of these meteorological phenomena are statistically different. We demonstrate using composites that, there is always a prevailing surface low-pressure along the northwestern bound of the AR which tends to form a confluence region. This confluence region coupled with positive PV anomalies and a prevalent mid-tropospheric trough serves as a good source of vertical and horizontal advection for water vapor. Guirguis et al. (2023) show in their work the impact of winds at the confluence region and their importance for moisture transport during different times in the DJF season. We find that during AR events in all ARDTs, there is more warmth in the column of intense IVT as compared to the surrounding meteorology which is consistent with the findings of Mo et al. (2022). The intensity of the IVT during ARs may depend on the strength of the some variables like the surface pressure gradients and mid tropospheric PV. Our results show that during CTs, there is higher IVT and TCWV, a stronger low-pressure anomaly, higher mid-tropospheric warm temperature anomaly, and a region of strong positive to negative PV anomaly gradient along the landfall region as opposed to the NCTs. These results are consistent with findings from Lora et al. (2020) andRutz et al. (2014) which suggests that the meteorology during CTs indicates synoptic conditions that are favorable for strong IVTs. PV on the other hand shows consistency in all 4 ARDTs; there is no statistical difference in the PV captured in all 4 ARDTs. Guirguis et al. (2019) using self-organizing maps (SOMs) shows that the different orientations of the 500 hPa heights could be a result of ENSO effects contributing to AR formation and landfall. The prevalence of the anomalous geopotential heights also has been identified to be influenced by the 4 Pacific North weather regimes, namely, the Alaskan Pacific, Baja Pacific, Canadian Pacific, and Off-shore California Pacific pressure systems. For the landfall site under consideration, Guirguis et al. (2023) show in their paper that all four modes come into play when ARs are prevalent

To ascertain the significance of the difference between ARDTs, the student's t-test is computed on the differences between ARDTs. We observe that during landfall, all ARDTs are statistically different from each other. Here, our goal is not to assess the phenomenon prior to landfall, however, results from this work point in the direction that, ARDTs could have different preceding meteorology like strong or weak atmospheric or oceanic frontal systems (Liu et al., 2021), strong confluence winds resulting from different sea level pressure magnitudes (Payne & Magnusdottir, 2016), and other meteorological phenomena which could lead to them identifying different frequencies and even, types of ARs.

Assessing the difference between prevailing atmospheric conditions for ARDTs has various implications and may lead to a better understanding of what physical processes to expect during AR events. Since observations are not able to quantify specifically the morphology of ARs, ARDTs are a good proxy to identify the point where a region of IVT can be classified as an AR, however, the definition of an AR may be subject to location and period. For instance, in a changing climate, the threshold for what may be defined as an AR that leads to extreme events may change since our threshold for classifying what an extreme is may also change. This is also mentioned in the study of O'Brien et al. (2022) where they observe that the uncertainty associated with ARDTs dominates that of models. Also, in a changing climate where water vapor increases, absolute ARDTs will become more permissive because the current absolute thresholds may not be a good definition for an AR. This brings to light questions like (1) Do these ARDTs continue to detect ARs associated with similar phenomena as the climate changes? (2) Since ARs are often associated with extratropical cyclones (ETCs), how often do ARDTs actually capture ETC-induced ARs? This work shows that we are able to observe similarities in the prevailing weather patterns during an AR, however, ARDTs may have different magnitudes associated with their atmospheric composites. This suggests that for any ARDT, the effects of ARs leading to extremes will be different and as a result, capturing AR-induced extremes may be subject to which ARDT is being analyzed. In light of this, future work will involve assessing landfalling ARs in different locations globally to ascertain if the prevailing weather patterns would remain the same in all instances.

Appendix A Supplemental Plots

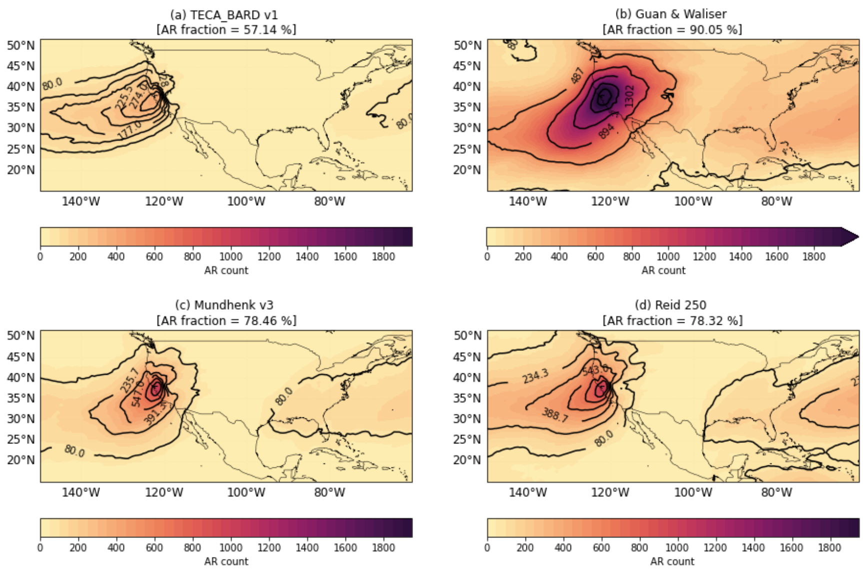

Figure A1. Non-Consensus times for land-falling ARs for all ARDTs. TECA_BARD v1 (a), Guan & Waliser (b), Mundhenk (c), Reid 250 (d). Percentages show the ratio of NCTs to the total AR frequency.

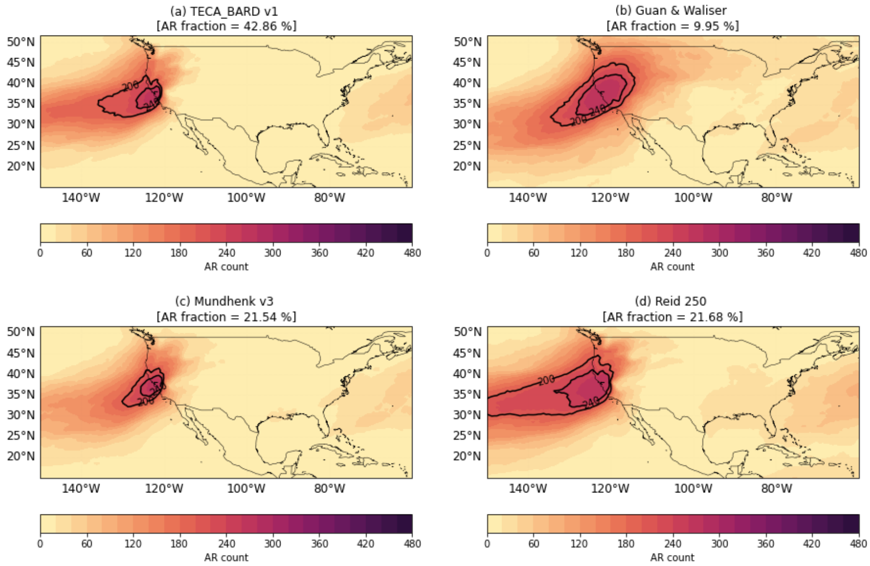

Figure A2. Consensus times for land-falling ARs for all ARDTs. TECA_BARD v1 (a), Guan & Waliser (b), Mundhenk (c), Reid 250 (d). Percentages show the ratio of CTs to the total AR frequencies.

Acknowledgments

This material is based upon work supported by the U.S. Department of Energy, Office of Science, Office of Biological and Environmental Research, Climate and Environmental Sciences Division, Regional & Global Model Analysis Program and used resources of the National Energy Research Scientific Computing Center (NERSC), also supported by the Office of Science of the U.S. Department of Energy under Contract No. DE-AC02-05CH11231. This research was supported in part by Lilly Endowment, Inc., through its support for the Indiana University Pervasive Technology Institute.

References

Bao, J., Michelson, S., Neiman, P., Ralph, F., & Wilczak, J. (2006). Interpretation of enhanced integrated water vapor bands associated with extratropical cyclones: Their formation and connection to tropical moisture. *Monthly weather review*, *134*(4), 1063–1080.

Barth, N. A., Villarini, G., Nayak, M. A., & White, K. (2017). Mixed populations and annual flood frequency estimates in the western united states: The role of atmospheric rivers. *Water Resources Research*, *53*(1), 257–269.

Blamey, R., Ramos, A., Trigo, R., Tomé, R., & Reason, C. (2018). The influence of atmospheric rivers over the south atlantic on winter rainfall in south africa. *Journal of Hydrometeorology*, *19*(1), 127–142.

Bluestein, H. B. (1992). *Synoptic-dynamic meteorology in midlatitudes: Observations and theory of weather systems* (Vol. 2). Taylor & Francis.

Dettinger, M. (2011). Climate change, atmospheric rivers, and floods in california–a multimodel analysis of storm frequency and magnitude changes 1. *JAWRA*

Journal of the American Water Resources Association, *47*(3), 514–523.
Dettinger, M. D. (2013). Atmospheric rivers as drought busters on the us west coast. *Journal of Hydrometeorology*, *14*(6), 1721–1732.
Dhana Laskhmi, D., & Satyanarayana, A. (2020). Climatology of landfalling atmospheric rivers and associated heavy precipitation over the indian coastal regions. *International Journal of Climatology*, *40*(13), 5616–5633.
Doiteau, B., Dournaux, M., Montoux, N., & Baray, J.-L. (2021). Atmospheric rivers and associated precipitation over france and western europe: 1980–2020 climatology and case study. *Atmosphere*, *12*(8), 1075.
Gelaro, R., McCarty, W., Suárez, M. J., Todling, R., Molod, A., Takacs, L., ... others (2017). The modern-era retrospective analysis for research and applications, version 2 (merra-2). *Journal of climate*, *30*(14), 5419–5454.
Gershunov, A., Shulgina, T., Clemesha, R. E., Guirguis, K., Pierce, D. W., Dettinger, M. D., ... others (2019). Precipitation regime change in western north america: the role of atmospheric rivers. *Scientific reports*, *9*(1), 9944.
Gershunov, A., Shulgina, T., Ralph, F. M., Lavers, D. A., & Rutz, J. J. (2017). Assessing the climate-scale variability of atmospheric rivers affecting western north america. *Geophysical Research Letters*, *44*(15), 7900–7908.
Goldenson, N., Leung, L., Bitz, C. M., & Blanchard-Wrigglesworth, E. (2018). Influence of atmospheric rivers on mountain snowpack in the western united states. *Journal of Climate*, *31*(24), 9921–9940.
Gonzales, K. R., Swain, D. L., Barnes, E. A., & Diffenbaugh, N. S. (2020). Moisture-versus wind-dominated flavors of atmospheric rivers. *Geophysical Research Letters*, *47*(23), e2020GL090042.
Guan, B., Molotch, N. P., Waliser, D. E., Fetzer, E. J., & Neiman, P. J. (2010). Extreme snowfall events linked to atmospheric rivers and surface air temperature via satellite measurements. *Geophysical Research Letters*, *37*(20).
Guan, B., & Waliser, D. E. (2015). Detection of atmospheric rivers: Evaluation and application of an algorithm for global studies. *Journal of Geophysical Research: Atmospheres*, *120*(24), 12514–12535.
Guirguis, K., Gershunov, A., Hatchett, B., Shulgina, T., DeFlorio, M. J., Subramanian, A. C., ... others (2023). Winter wet–dry weather patterns driving atmospheric rivers and santa ana winds provide evidence for increasing wildfire hazard in california. *Climate Dynamics*, *60*(5-6), 1729–1749.
Guirguis, K., Gershunov, A., Shulgina, T., Clemesha, R. E., & Ralph, F. M. (2019). Atmospheric rivers impacting northern california and their modulation by a variable climate. *Climate Dynamics*, *52*, 6569–6583.
Hagos, S., Leung, L. R., Yang, Q., Zhao, C., & Lu, J. (2015). Resolution and dynamical core dependence of atmospheric river frequency in global model simulations. *Journal of Climate*, *28*(7), 2764–2776.
Hersbach, H., Bell, B., Berrisford, P., Hirahara, S., Horányi, A., Muñoz-Sabater, J., ... others (2020). The era5 global reanalysis. *Quarterly Journal of the Royal Meteorological Society*, *146*(730), 1999–2049.
Inda-Díaz, H. A., O'Brien, T. A., Zhou, Y., & Collins, W. D. (2021). Constraining and characterizing the size of atmospheric rivers: A perspective independent from the detection algorithm. *Journal of Geophysical Research: Atmospheres*, *126*(16), e2020JD033746.
Jankov, I., Bao, J.-W., Neiman, P. J., Schultz, P. J., Yuan, H., & White, A. B. (2009). Evaluation and comparison of microphysical algorithms in arw-wrf model simulations of atmospheric river events affecting the california coast. *Journal of Hydrometeorology*, *10*(4), 847–870.
Junker, N. W., Grumm, R. H., Hart, R., Bosart, L. F., Bell, K. M., & Pereira, F. J. (2008). Use of normalized anomaly fields to anticipate extreme rainfall in the mountains of northern california. *Weather and forecasting*, *23*(3), 336–356.
Kashinath, K., Mudigonda, M., Kim, S., Kapp-Schwoerer, L., Graubner, A., Karais-

mailoglu, E., ... others (2021). Climatenet: an expert-labeled open dataset and deep learning architecture for enabling high-precision analyses of extreme weather. *Geoscientific Model Development*, *14*(1), 107–124.

Kim, H.-M., Zhou, Y., & Alexander, M. A. (2019). Changes in atmospheric rivers and moisture transport over the northeast pacific and western north america in response to enso diversity. *Climate Dynamics*, *52*(12), 7375–7388.

Kunkel, K. E., & Champion, S. M. (2019). An assessment of rainfall from hurricanes harvey and florence relative to other extremely wet storms in the united states. *Geophysical Research Letters*, *46*(22), 13500–13506.

Lamjiri, M. A., Dettinger, M. D., Ralph, F. M., & Guan, B. (2017). Hourly storm characteristics along the us west coast: Role of atmospheric rivers in extreme precipitation. *Geophysical Research Letters*, *44*(13), 7020–7028.

Lavers, D. A., & Villarini, G. (2015). The contribution of atmospheric rivers to precipitation in europe and the united states. *Journal of Hydrology*, *522*, 382–390.

Lavers, D. A., Villarini, G., Allan, R. P., Wood, E. F., & Wade, A. J. (2012). The detection of atmospheric rivers in atmospheric reanalyses and their links to british winter floods and the large-scale climatic circulation. *Journal of Geophysical Research: Atmospheres*, *117*(D20).

Leung, L. R., & Qian, Y. (2009). Atmospheric rivers induced heavy precipitation and flooding in the western us simulated by the wrf regional climate model. *Geophysical research letters*, *36*(3).

Liu, X., Ma, X., Chang, P., Jia, Y., Fu, D., Xu, G., ... Patricola, C. M. (2021). Ocean fronts and eddies force atmospheric rivers and heavy precipitation in western north america. *Nature communications*, *12*(1), 1268.

Lora, J. M., Mitchell, J. L., Risi, C., & Tripati, A. E. (2017). North pacific atmospheric rivers and their influence on western north america at the last glacial maximum. *Geophysical Research Letters*, *44*(2), 1051–1059.

Lora, J. M., Shields, C., & Rutz, J. (2020). Consensus and disagreement in atmospheric river detection: Artmip global catalogues. *Geophysical Research Letters*, *47*(20), e2020GL089302.

Mahoney, K., Jackson, D. L., Neiman, P., Hughes, M., Darby, L., Wick, G., ... Cifelli, R. (2016). Understanding the role of atmospheric rivers in heavy precipitation in the southeast united states. *Monthly Weather Review*, *144*(4), 1617–1632.

McIntyre, M. E. (2003). Potential vorticity. *Encyclopedia of atmospheric sciences*, *2*, 685–694.

Mo, R., Lin, H., & Vitart, F. (2022). An anomalous warm-season trans-pacific atmospheric river linked to the 2021 western north america heatwave. *Communications Earth & Environment*, *3*(1), 1–12.

Mundhenk, B. D., Barnes, E. A., & Maloney, E. D. (2016). All-season climatology and variability of atmospheric river frequencies over the north pacific. *Journal of Climate*, *29*(13), 4885–4903.

Nayak, M. A., Villarini, G., & Lavers, D. A. (2014). On the skill of numerical weather prediction models to forecast atmospheric rivers over the central united states. *Geophysical Research Letters*, *41*(12), 4354–4362.

Neiman, P. J., Ralph, F. M., Wick, G. A., Lundquist, J. D., & Dettinger, M. D. (2008). Meteorological characteristics and overland precipitation impacts of atmospheric rivers affecting the west coast of north america based on eight years of ssm/i satellite observations. *Journal of Hydrometeorology*, *9*(1), 22–47.

O'Brien, T. A., Risser, M. D., Loring, B., Elbashandy, A. A., Krishnan, H., Johnson, J., ... others (2020). Detection of atmospheric rivers with inline uncertainty quantification: Teca-bard v1. 0.1. *Geoscientific Model Development*, *13*(12), 6131–6148.

O'Brien, T. A., Wehner, M. F., Payne, A. E., Shields, C. A., Rutz, J. J., Leung, L.-R., ... others (2022). Increases in future ar count and size: Overview of the artmip tier 2 cmip5/6 experiment. *Journal of Geophysical Research: Atmospheres*, *127*(6), e2021JD036013.

Pan, M., & Lu, M. (2019). A novel atmospheric river identification algorithm. *Water Resources Research*, *55*(7), 6069–6087.

Payne, A. E., & Magnusdottir, G. (2014). Dynamics of landfalling atmospheric rivers over the north pacific in 30 years of merra reanalysis. *Journal of Climate*, *27*(18), 7133–7150.

Payne, A. E., & Magnusdottir, G. (2015). An evaluation of atmospheric rivers over the north pacific in cmip5 and their response to warming under rcp 8.5. *Journal of Geophysical Research: Atmospheres*, *120*(21), 11–173.

Payne, A. E., & Magnusdottir, G. (2016). Persistent landfalling atmospheric rivers over the west coast of north america. *Journal of Geophysical Research: Atmospheres*, *121*(22), 13–287.

Ralph, F., Coleman, T., Neiman, P., Zamora, R., & Dettinger, M. (2013). Observed impacts of duration and seasonality of atmospheric-river landfalls on soil moisture and runoff in coastal northern california. *Journal of Hydrometeorology*, *14*(2), 443–459.

Ralph, F. M., & Dettinger, M. D. (2011). Storms, floods, and the science of atmospheric rivers. *Eos, Transactions American Geophysical Union*, *92*(32), 265–266.

Ralph, F. M., Neiman, P. J., & Wick, G. A. (2004). Satellite and caljet aircraft observations of atmospheric rivers over the eastern north pacific ocean during the winter of 1997/98. *Monthly Weather Review*, *132*(7), 1721–1745.

Ralph, F. M., Rutz, J. J., Cordeira, J. M., Dettinger, M., Anderson, M., Reynolds, D., ... Smallcomb, C. (2019). A scale to characterize the strength and impacts of atmospheric rivers. *Bulletin of the American Meteorological Society*, *100*(2), 269–289.

Reid, K. J., King, A. D., Lane, T. P., & Short, E. (2020). The sensitivity of atmospheric river identification to integrated water vapor transport threshold, resolution, and regridding method. *Journal of Geophysical Research: Atmospheres*, *125*(20), e2020JD032897.

Rutz, J. J., Shields, C. A., Lora, J. M., Payne, A. E., Guan, B., Ullrich, P., ... Viale, M. (2019a). The atmospheric river tracking method intercomparison project (artmip): Quantifying uncertainties in atmospheric river climatology. *Journal of Geophysical Research: Atmospheres*, *124*(24), 13777-13802. Retrieved from `https://agupubs.onlinelibrary.wiley.com/doi/abs/10.1029/2019JD030936` doi: https://doi.org/10.1029/2019JD030936

Rutz, J. J., Shields, C. A., Lora, J. M., Payne, A. E., Guan, B., Ullrich, P., ... others (2019b). The atmospheric river tracking method intercomparison project (artmip): quantifying uncertainties in atmospheric river climatology. *Journal of Geophysical Research: Atmospheres*, *124*(24), 13777–13802.

Rutz, J. J., & Steenburgh, W. J. (2012). Quantifying the role of atmospheric rivers in the interior western united states. *Atmospheric Science Letters*, *13*(4), 257–261.

Rutz, J. J., Steenburgh, W. J., & Ralph, F. M. (2014). Climatological characteristics of atmospheric rivers and their inland penetration over the western united states. *Monthly Weather Review*, *142*(2), 905–921.

Ryoo, J.-M., Kaspi, Y., Waugh, D. W., Kiladis, G. N., Waliser, D. E., Fetzer, E. J., & Kim, J. (2013). Impact of rossby wave breaking on us west coast winter precipitation during enso events. *Journal of Climate*, *26*(17), 6360–6382.

Shields, C. (2019). *Artmip tier 1 catalogues. ucar/ncar - climate and global dynamics laboratory.* https://doi.org/10.5065/D6R78D1M. (Accessed 06 February 2023)

Shields, C. A., Payne, A. E., Shearer, E. J., Wehner, M. F., O'Brien, T. A., Rutz, J. J., ... others (2023). Future atmospheric rivers and impacts on precipitation: Overview of the artmip tier 2 high-resolution global warming experiment. *Geophysical Research Letters*, *50*(6), e2022GL102091.

Shields, C. A., Rutz, J. J., Leung, L.-Y., Ralph, F. M., Wehner, M., Kawzenuk, B., . . . others (2018). Atmospheric river tracking method intercomparison project (artmip): project goals and experimental design. *Geoscientific Model Development*, *11*(6), 2455–2474.

Turner, J., Lu, H., King, J. C., Carpentier, S., Lazzara, M., Phillips, T., & Wille, J. (2022). An extreme high temperature event in coastal east antarctica associated with an atmospheric river and record summer downslope winds. *Geophysical Research Letters*, *49*(4), e2021GL097108.

Williams, A. P., Cook, E. R., Smerdon, J. E., Cook, B. I., Abatzoglou, J. T., Bolles, K., . . . Livneh, B. (2020). Large contribution from anthropogenic warming to an emerging north american megadrought. *Science*, *368*(6488), 314–318.

Xiong, Y., & Ren, X. (2021). Influences of atmospheric rivers on north pacific winter precipitation: Climatology and dependence on enso condition. *Journal of Climate*, *34*(1), 277–292.

Zhang, J., Jia, Y., Ji, R., & Wu, Y. (2021). Decadal variation of atmospheric rivers in relation to north atlantic tripole sst mode. *Atmosphere*, *12*(10), 1252.

Zhou, T.-J., & Yu, R.-C. (2005). Atmospheric water vapor transport associated with typical anomalous summer rainfall patterns in china. *Journal of Geophysical Research: Atmospheres*, *110*(D8).

Zhou, Y., O'Brien, T. A., Collins, W. D., Shields, C. A., Loring, B., & Elbashandy, A. A. (2022). Characteristics and variability of winter northern pacific atmospheric river flavors. *Journal of Geophysical Research: Atmospheres*, *127*(23), e2022JD037105.

Zhu, Y., & Newell, R. E. (1998). A proposed algorithm for moisture fluxes from atmospheric rivers. *Monthly weather review*, *126*(3), 725–735.

Similarities in Meteorological Composites Among Different Atmospheric River Detection Tools During Atmospheric River Landfall.

Kwesi T. Quagraine [1], Travis A. O'Brien [1,2], Mohammad Rubaiat Islam [1]

[1]Earth and Atmospheric Science Department, Indiana University Bloomington, USA
[2]Climate and Ecosystem Sciences Division, Lawrence Berkeley National Laboratory, Berkeley, CA, USA

Key Points:

- The four ARDTs assessed predominantly capture similar atmospheric processes, however, with statistically significant difference in magnitudes.
- Landfalling ARs have a prevalent low-pressure and high-pressure confluence that enhance moisture influx toward the AR landfalling site.
- During consensus times, IVTs are higher as compared to non-consensus times.

Corresponding author: Travis A. O'Brien, `obrienta@iu.edu`

Abstract

Many atmospheric river detectors (ARDTs) have been developed over the past few decades to capture atmospheric rivers (ARs). However, different ARDTs have been observed to capture different frequencies, shapes and sizes of ARs. Due to this, many questions including investigating the underlying phenomena for ARs in the ARDTs have been posed. In this paper, we assess four different ARDTs and investigate the underlying meteorological phenomena during landfalling ARs. We find that during landfalling ARs events, there exists a prevalent low-pressure and high-pressure confluence that enhances moisture influx toward the landfalling site. The strength of the pressure gradient in the confluence region enhances the influx of the integrated vapor transport. The four ARDTs predominantly capture similar atmospheric processes, nonetheless, they have statistically different magnitudes.

Plain Language Summary

Atmospheric rivers (ARs) are an atmospheric phenomena that is responsible for transporting water vapor from the warm tropics to the cold polar regions. As they transport, they rain out the transported water vapor. Due to their influence on precipitation, researchers have developed different methods in tracking them. In an attempt to track them, it is observed that the different AR identification methods capture different frequencies and sizes during AR propagation and landfall. These differences have raised questions concerning the prevailing meteorological phenomena during ARs. In this paper, we assess four ARDTs during landfalling AR events and investigate their prevailing meteorological phenomena. We find that all four ARDTs predominantly capture similar meteorological phenomena, however, with statistically different magnitudes.

1 Introduction

Atmospheric rivers (ARs) are a type of weather phenomenon that is important for moving water from the warm, moist tropics to the cool dry polar regions (Zhu & Newell, 1998; Guan et al., 2010; M. Dettinger, 2011; F. M. Ralph & Dettinger, 2011; O'Brien et al., 2020). ARs are associated with storm tracks and result in extreme winds, and substantial amounts of precipitation which result in floods and large snow packs (M. D. Dettinger, 2013; M. Dettinger, 2011; Neiman et al., 2008; F. M. Ralph & Dettinger, 2011; Payne & Magnusdottir, 2014; Guan et al., 2010). The literature shows that about 40% of high precipitation events on the west Indian coast (Dhana Laskhmi & Satyanarayana, 2020) and ∼70% of heavy precipitation events over South Africa (Blamey et al., 2018) are associated with ARs. Over the Western U.S. and other water-stressed areas, weak ARs produce beneficial rain and snow that is an important source of freshwater (Guan et al., 2010; M. Dettinger, 2011; Rutz & Steenburgh, 2012; Kunkel & Champion, 2019) and may be a relief for drought conditions in some regions (M. D. Dettinger, 2013). Over the west coast of North America, studies have shown that ARs contribute to precipitation as much as 15 to 35% over southern California and about 25 to 60% over coastal Washington (M. Dettinger, 2011; Rutz et al., 2014; Guan & Waliser, 2015). In summary, ARs contribute about 50% of the total annual precipitation over North America (Gershunov et al., 2019). Although these AR-induced precipitations sometimes alleviate water stress over the region, some of these precipitation events have led to extreme precipitation events. (Lamjiri et al., 2017; Barth et al., 2017). In the western United States of America (USA), it is projected that the number of AR-induced extreme precipitation events may increase whereas the overall frequency of non-AR-related precipitation may decrease (Lavers & Villarini, 2015; Williams et al., 2020). Although all other AR-prone regions in the world are not spared of these AR-induced extreme events, this work focuses on AR events in the northern Pacific basin due to the well-documented impacts once they make landfall over the region (Payne & Magnusdottir, 2014; F. M. Ralph et al., 2019).

Although the literature shows a clear association between ARs and extreme precipitation events (Barth et al., 2017; F. M. Ralph et al., 2019), recent studies have started associating ARs with extreme heat events. Such events include the summer heat wave event over the northwestern coast of North America in 2021 (Mo et al., 2022). In this event, there were record-breaking temperatures of about 46 ^{o}C. This resulted in heat strokes and other heat-related diseases in the region (Mo et al., 2022). Also, an extreme high-temperature event recorded over coastal East Antarctica in 1989 has recently been attributed to AR influx into the region (Turner et al., 2022). Turner et al. (2022) show in their findings that "Sustained horizontal warm advection toward the coast of East Antarctic via an atmospheric river led to the marked warming".

The effects associated with ARs have led to a large amount of research on AR frequency, intensity, variability, and change (M. Dettinger, 2011; Mundhenk et al., 2016; Lavers & Villarini, 2015); others have investigated AR morphology and other aspects of AR evolution including size, water content, windiness, et cetera (Payne & Magnusdottir, 2015, 2016; Doiteau et al., 2021). Other research has investigated the correlations between signatures of ARs and climate model indices (like El- Niño Southern Oscillation (ENSO) and Madden-Julian Oscillation(MJO)) and observed that ENSO modulates the latitude of landfalling ARs. Also, most landfalling AR dates occur during El Niño. The MJO is shown to modulate the intensity of landfalling ARs, as well as precipitation totals(Payne & Magnusdottir, 2014). Payne and Magnusdottir (2014); Neiman et al. (2008) have also investigated AR dynamics and have shown that during ARs there is a synoptic scale low pressure on the northwestern side and a high pressure on the southeastern side of the region of intense IVT characterized as the AR. Also, ARs have been associated with frontal boundaries; both oceanic and atmospheric fronts (Xiong & Ren, 2021; Neiman et al., 2008). Other research suggests that some ARs form in association with the warm conveyor belt of extratropical cyclones and they may not necessarily be associated with just one cyclone but can span the lifetimes of multiple cyclones (Payne & Magnusdottir, 2014). Ryoo et al. (2013) found that moisture transport in ARs is somewhat modulated by the subtropical jet and also the location of the Rossby wave breaking along the west coast of North America. In an attempt to understand AR morphology, Payne and Magnusdottir (2014) have also shown that ARs have an association with Rossby waves. Their findings also conclude that ARs are modulated by the influence of the tropical on the extratropical but their variability is more strongly tied to extratropical dynamics than tropical dynamics. The co-occurrence of ARs with other phenomena such as Pacific Decadal Oscillation (PDO) (Gershunov et al., 2017) and Arctic Multidecadal Oscillations (AMO) (Zhang et al., 2021) have been investigated in the literature. One understudied phase of these experiments to understand ARs is that most of the various planetary scale phenomena research was conducted using one ARDT, therefore suggesting that we should consider an ensemble of ARDTs to investigate if these findings are true for all ARDTs.

Studies over the years have looked at different methods to categorize, track, and count the number of ARs in the atmosphere at any given time (O'Brien et al., 2020; Inda-Díaz et al., 2021; Guan & Waliser, 2015; Lavers et al., 2012). From region to region, the availability of water vapor, wind speeds and direction, geopotential height, jet stream location and phase speeds, vertical profile, and many other meteorological variables may play a substantial role in the genesis, evolution, transport, landfall, and breaking of the AR (F. Ralph et al., 2013; F. M. Ralph et al., 2004; Bao et al., 2006; Jankov et al., 2009; Guan & Waliser, 2015). Scientists have developed different metrics or algorithms for characterizing ARs using these meteorological variables. Basically, most atmospheric river detectors (ARDTs) are a set of algorithms that set a threshold on the spatial extent and water vapor transport in the troposphere and call them atmospheric river objects. Due to the vast number of ARDTs being developed, the Atmospheric Rivers Tracking Method Intercomparison Project was started with the aim of collating and investigating the experimental designs of various AR algorithms (Rutz et al., 2019a).

Since the inception of ARTMIP, many ARDTs have been collated and implemented on a specific common dataset for a defined period of time. The ARTMIP project comprises two phases (i.e, Tier 1 which uses the Modern Era Retrospective-analysis for Research and Applications (MERRA - 2) as a baseline for comparisons, and Tier 2 which includes sensitivity studies designed around specific scientific questions (C. A. Shields et al., 2018; O'Brien et al., 2020). Although all these ARDTs use similar datasets, they have different levels of "permissiveness" as to what should be characterized as an AR. This permissiveness leads to differences in their AR frequencies, intensities, duration, and attribution of high-impact weather and climate events to ARs (C. A. Shields et al., 2018; Lora et al., 2020).

More often than not, AR detection studies use either the integrated water vapor (IWV) like Goldenson et al. (2018); Hagos et al. (2015); Kashinath et al. (2021) or the integrated vapor transport (IVT) like Leung and Qian (2009); Lora et al. (2017); Mahoney et al. (2016) and many others. These variables (IVT and IWV) over the years have been assessed to know which of them gives a better characteristic for AR detection and attribution. Junker et al. (2008) and F. Ralph et al. (2013) in their work show that IVT is more strongly correlated with cool season precipitation as compared to IWV. IVT also penetrates further inland and is spatially co-located with regions of precipitation more than IWV. Due to the difference in variable preference and thresholding values for these variables (i.e., IVT and IWV), ARDTs capture different frequencies, intensities, and structures of ARs. Therefore some researchers clearly state their preference to use IVT as opposed to IWV (Nayak et al., 2014; Rutz et al., 2014).

Aside from the disparities in IVT or IWV selection and preference based on specific scenarios, the basic idea for AR detection is the use of IVT or IWV thresholds. Some studies either use an absolute categorization method – a specific threshold is set for all instances – or a relative categorization method – the threshold changes based on an event. Other ARDTs also use tracking algorithms. In these tracking algorithms, a Lagrangian-style detection is used, where ARs are considered as objects being tracked. For instance Lavers et al. (2012) use the median IWV percentile as the threshold for categorizing ARs over western Europe, Kashinath et al. (2021) use machine learning based on segmentation, trained on 500 expert labeled images to track AR associated extreme events. Lora et al. (2017) use Integrated Vapor Transport that is 100 $kgm^{-1}s^{-1}$ above climatological area means for North Pacific as a criterion for categorizing ARs. These and many other ways have been used to categorize ARs in literature. Although IVT and IWV are the main components of detecting ARs, there are other atmospheric parameters that are sometimes coupled with these two due to their supposed influence on the detection algorithms. In Lora et al. (2017) winds and precipitation are included in their detection of ARs. Many of these differences in literature lead to the question: Do all ARDTs observe similar weather phenomena when they detect ARs?

The methods for detecting ARs have proved to be fundamentally consistent with each other on what we "normally" classify as an AR (C. A. Shields et al., 2023), however, ARDTs capture these AR objects in different frequencies, intensities, shapes, and sizes (Inda-Díaz et al., 2021; C. A. Shields et al., 2018; Rutz et al., 2019b). In this work, we investigate the underlying meteorological phenomena that govern a specific set of ARDTs and hypothesis that different ARDTs capture different meteorological phenomena during AR landfall. This hypothesis stems from evidence that different ARDTs capture different frequencies (C. A. Shields et al., 2018) of ARs and, as such, may have different weather conditions during AR detection for any given ARDT. Also, the intensity of these captured ARs would depend on the weather preceding the AR. Therefore, this work seeks to characterize the meteorological phenomena associated with four commonly used ARDTs and investigate the meteorological phenomena associated with the intensity and frequency of the occurrence of the ARs in the specific ARDT over the west coast of the United States.

2 Method

In this work we attempt to identify different weather phenomena that are associated with different ARDTs. In so doing, we use specific AR-related variables like potential vorticity, total column of water vapor, IVT, geopotential heights, temperature, and mean sea level pressure. These variables are selected due to their suggested influence on moisture transport and general atmospheric circulation (T.-J. Zhou & Yu, 2005; Bao et al., 2006; Kim et al., 2019). We focus on the December-February (DJF) period. Climatologically, over the west coast of the US, the impacts of ARs that make landfall along the area are mostly within this period (Neiman et al., 2008; Payne & Magnusdottir, 2014; F. Ralph et al., 2013; Mundhenk et al., 2016).

2.0.1 Consensus Times (CT) and Non-consensus Times (NCT)

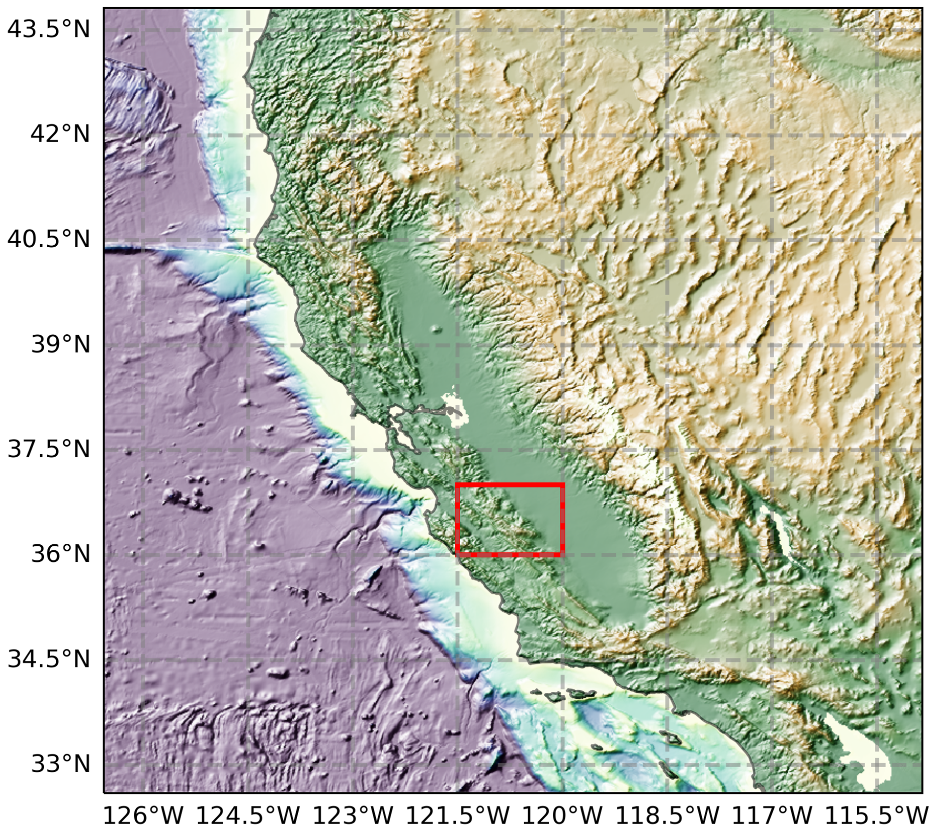

Figure 1. Map of the west coast of the United States of America. The red box represents the landfalling AR region selected to show consensus.

To independently select land falling ARs that are representative of the various algorithms, a region which is well impacted by ARs (M. Dettinger, 2011; Neiman et al., 2008), is selected along the west coast of the Continental United States (CONUS), and the frequency of landfalling ARs over the region (red box in Figure 1) are captured. Consensus times (CT), which are times where all ARDTs captured ARs are grouped apart from non-consensus times (NCT). By definition, these consensus times have the same phenomena for all algorithms under study since the meteorology at those timesteps is from the same datasets. NCTs are days that do not coincide in all four ARDTs. This means there is a probability of some days being alike in 2 or 3 algorithms however, they are not recognized as CT days because they do not meet the criteria of consensus (that is, all 4 algorithms must capture that time).

2.0.2 Anomaly

Anomalies (deviations from the climatology) are computed for the NCT ARs using the climatologies from the DJF season since the focus of ARs in this study is in that season. To compute the climatology, the DJF season (winter) for the entire temporal regime is selected and the mean is computed using this sample. Spatial anomalies show the magnitude of change of a variable from its climatology at a data point. This is computed as

$$\bar{V} = \frac{1}{M}\sum_{i}^{J} X_i \qquad \{where\ X_i \in NCTs\ or\ CTs\} \tag{1}$$

$$\bar{V}^y = \frac{1}{N}\sum_{i}^{J} Y_j \qquad \{where\ Y_j \in DJF\ in\ every\ year\} \tag{2}$$

$$V_{anom} = \bar{V} - \bar{V}^y \tag{3}$$

where $\bar{V}$ is the average CT or NCTs captured in an ARDT and $\bar{V}^y$ is the climatological mean of DJFs every year.

2.0.3 Bootstrapping

To test the significance of the anomaly, bootstrapping is used to test the null hypothesis that all ARDTs capture ARs under the same meteorological phenomena and magnitude. If the null hypothesis is false, then differences in meteorological composites between two ARDTs should be statistically different from zero. We use a bootstrapping procedure, described in the next paragraph, to estimate the distribution of differences between NCT composites for each grid cell.

To formulate this bootstrapping test, we do the following. We randomly sample with replacement all timesteps in the datasets and compute the mean over time for every bootstrap sample. We repeat this random sampling process for 1000 bootstrap samples. These samples are concatenated into one dataset. The bias between the bootstrap ($\Delta = X_1^b - X_2^b$, where X_1^b and X_2^b represents bootstrapped datasets and Δ is the difference between 2 datasets) samples for the algorithms is computed. This bias, if centered around 0 shows that the results between 2 specific algorithms are not statistically different for a specific atmospheric variable. However, if the bias between the samples is different from 0, then we use the student's t-test as the test for significance. This process is repeated for all variables and all gridcells to check the statistical significance of the phenomena being observed.

3 Data

We mostly use the ARTMIP database for obtaining the various ARDTs. In this catalog, AR detection algorithms were run using the same dataset for the derived variables, IWV and IVT from Modern-Era Retrospective Analysis for Research and Applications

(MERRA-2)(Gelaro et al., 2017). We consider the Tier 1 ARTMIP data catalog from 1980 to 2017 (C. A. Shields et al., 2018). Prior to ARTMIP, most AR algorithms used different datasets and were for specific regions, however, in ARTMIP Tier 1, the same datasets were used and also some algorithms were run for the entire globe (C. A. Shields et al., 2018). The ARTMIP catalog contains ARDTs computed on 3-hourly timescales and each grid point is tagged using binary indicators (0 for no AR presence and 1 for AR presence) (C. A. Shields et al., 2018). The catalog for the datasets can be found in C. Shields (2019).

Here, we focus mainly on 4 algorithms submitted to the ARTMIP Tier 1, that is, the Guan & Waliser (Guan & Waliser, 2015), Mundhenk v2 (Mundhenk et al., 2016), TECA BARD v1 (O'Brien et al., 2020) and the Reid250 (Reid et al., 2020) algorithms. These specific algorithms were chosen because they are all computed using the same variable (i.e., IVT, which inculcates the direction of flow in its calculation unlike the IWV which is the amount of water vapor in the atmosphere at a specific time) and most importantly, they cover the 3 major categories of ARDTs previously discussed: relative, absolute, and percentile-time detection.

To account for the meteorology associated with ARDTs, we consider the European Centre for Medium-Range Weather Forecast's (ECMWF) Reanalysis 5 (ERA5) dataset. We select a few of the variables which include the total column of water vapor (TCWV), IVT, mean sea level pressure (MSL), potential vorticity at 500 hPa (PV), geopotential heights at 500 hPa (GEOPTH) and 500 hPa temperature. These variables are selected based on their ability to detect most synoptic scale features that are associated with precipitable water, its transport, and the meteorology that occur during their existence (T.-J. Zhou & Yu, 2005; Bao et al., 2006; Kim et al., 2019). These quantities have proven to be representative of mid-latitude dynamics and are generally used in mid-latitude studies and textbooks (Bluestein, 1992; McIntyre, 2003). Also, past research hints at their importance for mid-latitudinal atmospheric transport (McIntyre, 2003). The ERA5 dataset has a spatial resolution of $0.25^o \times 0.25^o$ and a temporal resolution of 1 hour with 37 levels for atmospheric variables with levels. The entire duration of data considered in this study is from 1979 to 2017 (Hersbach et al., 2020).

4 Results

The results show that there are differences between ARDTs during CTs and NCTs (Table 1). Table 1 shows that TECA_BARD v1 (Guan & Waliser) is the most restrictive (permissive) ARDT among the four. TECA_BARD v1 (Guan & Waliser) has the least (highest) fraction of AR counts particular to it. These differences in frequencies are consistent with C. A. Shields et al. (2018) which reflects that there are differences in AR frequencies across ARDTs. Unique times where ARs are captured separately from any other ARDT show that TECA_BARD is the ARDT in the least disagreement with all other ARDTs on what describes an AR. Guan & Waliser is the algorithm with the highest disagreement as compared to other ARDTs. The spatial distribution of these frequencies can be seen in supplemental figures (SA1 and SA2).

We investigate some atmospheric variables to observe the spatial orientation of meteorology associated with the CTs of ARs. For CTs, Figures 2 (a) and (b) shows that in CTs there are large positive IVT anomalies ($\sim > 300$ kgm^{-2}s^{-2}), positive TCWV anomalies with the highest of ~ 10 kgm^{-2}, and generally warm 500 hP temperature anomalies ($\sim$ 4K) anomalies along the landfall region. This orientation of column variables is coupled with a low-pressure anomaly along the Aleutian low and a 500 hPa trough in the geopotential height. The atmospheric orientation shows a strong temperature gradient which has its low superimposed on the low-pressure anomaly over the Pacific Northwest (PNW) and the high-temperature anomaly over land.

	TECA_BARD v1	Guan & Waliser	Mundhenk v3	Reid 250
Consensus times (CTs)	279 (42.86%)	279 (9.95%)	279 (21.54%)	279 (21.68%)
Non-consensus times (NCTs)	379 (57.14%)	2526 (90.05%)	1016 (78.46%)	1008 (78.32%)
Total number of ARs	658	2805	1295	1287
Unique ARs	9 (1.38%)	1170 (41.71%)	34 (2.63 %)	88 (6.84%)

Table 1. Table showing the algorithms and the number of consensuses, Non-consensus, and unique ARs and their percentages with respect to the total number of ARs captured in an ARDT. Text in red represents the most restrictive (Consensus times) and most permissive (Non-consensus times).

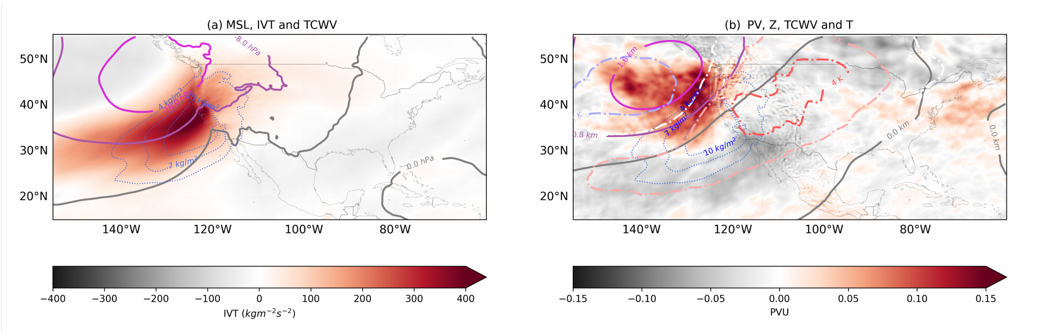

Figure 2. DJF Consensus times composites for atmospheric variables; IVT (grey, white, and red shading), MSL (magenta, grey, and dark red solid line), TCWV (blue dots) panel (a) and 500 hPa Potential Vorticity (grey, white, and red shading) 500 hPa temperature (blue white red dashed dot line) and 500 hP geopotential heights (magenta, grey, brown solid line) (b) [Red square represents the AR region]

Comparatively, the anomalies in the NCTs (Figure 4 and 3) are of smaller magnitudes as compared to the CTs (Figure 2). This suggests that all ARDTs are able to capture AR frequencies that have pronounced atmospheric conditions. In other words, the more extreme an AR is, the higher the possibility that an ARDT may capture it.

The ARDTs show different orientations of IVT along the landfall region (Figure 3). Unlike all other ARDTs, TECA_BARD v1 shows a more westerly flow of moisture. All ARDTs except TECA_BARD v1 have a cut-off of IVT anomaly right around the 0 hPa surface pressure anomaly. TECA_BARD v1 ARDT tends to capture more IVT within the AR column as compared to the other ARDTs. Over the 500 hPa level (Figure 4), the Guan & Waliser ARDT shows a cooler mid-column of IVT. The Reid 250 ARDT has the warmest mid-tropospheric column of ARs. Although the mid-troposphere for Reid 250 is warm, the highest warmth ($\sim$ 4K) is located about 5^o east from the landfalling region and also further dissociated from the column of high IVT anomaly. TECA_BARD however has the most elongated column of positive temperature anomaly. This is consistent with the results from Mo et al. (2022) who suggest that ARs are associated with tropospheric heating. TECA_BARD v1 is observed to have an entirely warm column of IVT over the landfall region and over the region of intense IVT anomaly (the AR column). The result from

TECA_BARD v1 compares well with CT's atmospheric patterns. This warm layer in TECA_BARD v1 is accompanied by positive 500 hPa height anomalies that are not observed in any of the ARDTs. The surface low-pressure anomaly (Figure 3) located on the Northwest of the landfall region for all ARDTs shows a corresponding upper-level (500 hPa) negative geopotential anomaly (Figure 4) in all ARDT.

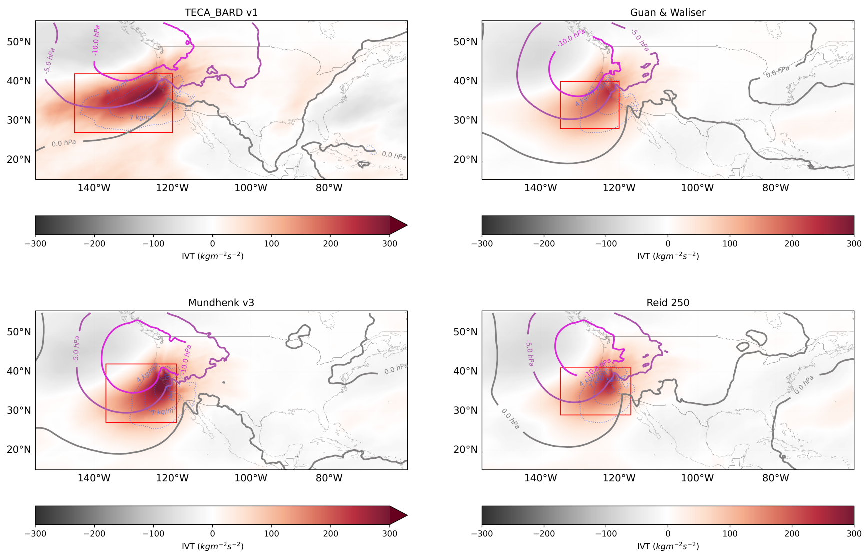

Figure 3. DJF Non-consensus times composites for atmospheric variables; IVT (grey, white, and red shading), MSL (magenta, grey, and dark red solid line), TCWV (blue dots) [Red square represents the AR region]

Over the landfalling region, we assess the difference in magnitudes of composites in Figure 5. Values of IVT and TCWV for TECA_BARD v1 are higher at the landfall site as compared to all other ARDTs, hence, the positive displacement of the PDF for any ARDT and TECA_BARD v1 difference. PV differences show that for all ARDTs, there is substantial instability which is observed in the positive PV anomalies. This implies there is expansion in the air column (warmth) and potential for rotation along the landfall region. TECA_BARD v1 tends to have the highest instability and rotation in the PV field. At the 500 hPa heights (Z plots), TECA_BARD v1 which has the warmest area within the landfall region also has the highest heights when compared with all other ARDTs.

The differences in the various magnitudes of composites for the ARDTs suggest that the differences are statistically significant for each ARDT. Figure 6 shows the significance plot for IVT between the ARDTs as the shading and the significance at 90%, 95%, and 99% levels. Over AR and landfalling region, there are statistically significant differences between all ARDTs. These differences are more pronounced in the MSL confluence region for all ARDTs. For all other variables assessed here, ARDTs show a statistically significant difference. This suggests although ARDTs may show similar spatial orientations (with slightly different spatial extents) of atmospheric phenomena during ARs, the magnitudes of atmospheric conditions for all ARDTs are statistically significantly dif-

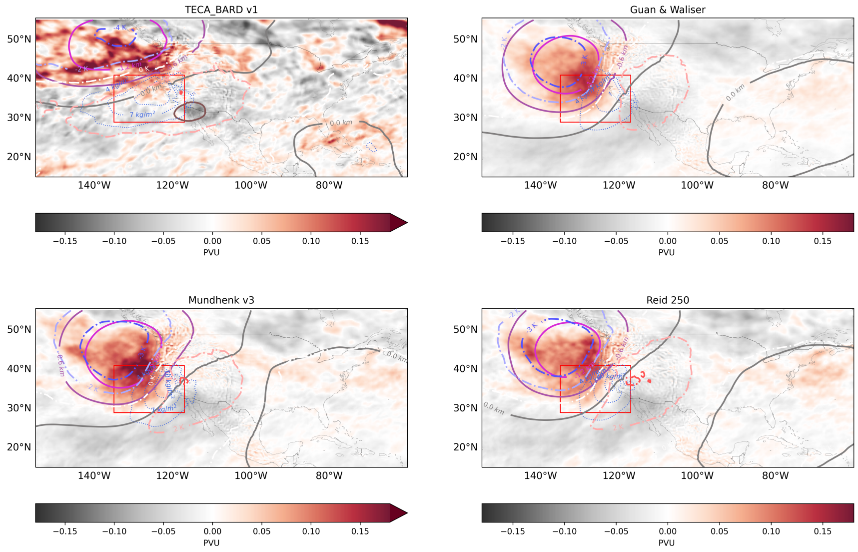

Figure 4. DJF Non-consensus times composites for atmospheric variables; Potential Vorticity (grey, white, and red shading) 500 hP temperature (blue white red dashed dot line) and 500 hP geopotential heights (magenta, grey, brown solid line) [Red square represents the AR region]

310 ferent from each other (see also supplementary figures). However, the difference in PV
311 anomalies for ARDTs did not show any statistical significance for all ARDTs.

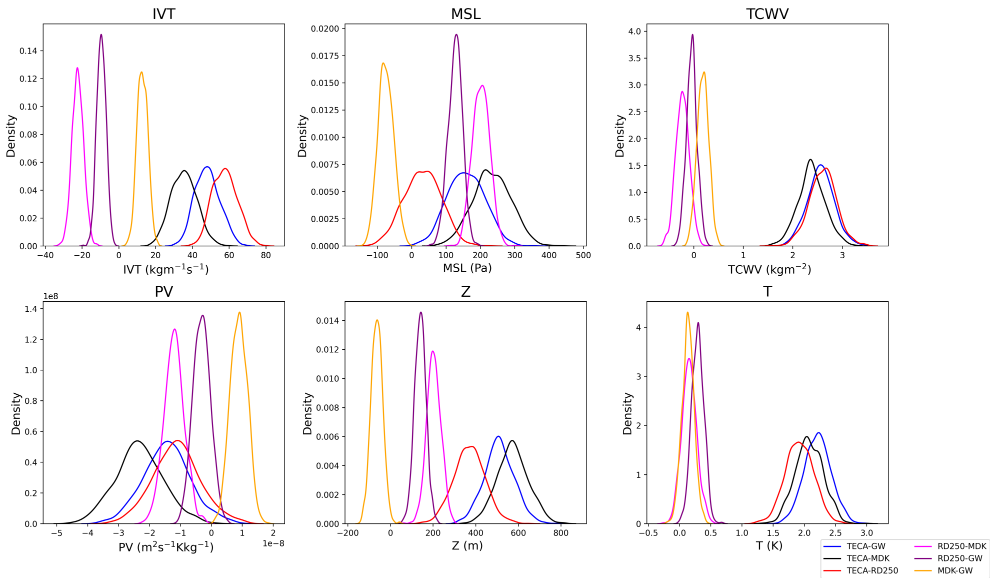

Figure 5. Probability distribution of differences in atmospheric variables for the various ARDTs between 145^{o}W to 118^{o}W and 25^{o}N to 45^{o}N

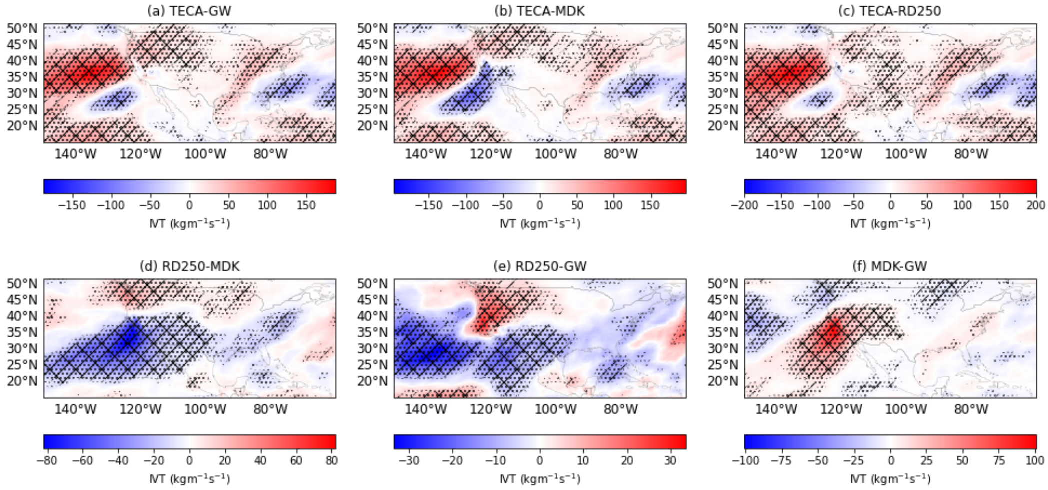

Figure 6. IVT difference plots between ARDTs (shading). Significance computed at 99% (/), 95% (//), and 90%(..) confidence intervals using the student t-test.

5 Summary and Discussion

ARs are proving to be more influential in mid-latitude weather than previously understood. Previous research (i.e., about 2 decades ago) has looked at the influence of precipitation caused by ARs, however, over the last decade, research has shown that ARs are not merely associated with precipitation, but also extreme precipitation and some heat waves (Liu et al., 2021; O'Brien et al., 2022; Mo et al., 2022). One may argue that these effects may not be well represented in all ARDTs, which may be true due to the preference for detection. For permissive ARDTs, these signals of extreme precipitation may be reduced in composite precipitation data as opposed to restrictive ARDTs. Here, we have looked at using different ARDTs which have different levels of permissiveness to assess the meteorology behind ARs during landfall. Using single ARDTs could be beneficial for specific regions based on the method of AR categorization. For instance, Guan & Waliser would be good for studies along tropical regions because it is not latitudinally filtered (Guan & Waliser, 2015), whereas TECA_BARD v1 may not be a good choice for tropical regions because of its Gaussian latitudinal filter (O'Brien et al., 2020) used to dampen the Inter Tropical Convergence Zone (ITCZ) and as a result, captures stronger ARs as seen in Figure 3, the use of the Mundhenk algorithm may be beneficial for characterizing ARs specific to time and location since they use a time and spatially varying percentile categorization (Mundhenk et al., 2016), the Pan and Lu (2019) algorithm uses both a local and global filter to make the capture of ARs in the polar regions more characteristic of the region due to lower water vapor presence in the region as opposed to other parts of the globe where there is substantial water vapor. These different algorithm structures and detection mechanisms show the potential difference in frequency, intensity, and duration of ARs. So in our work, we use these different ARDTs over a region where they all capture ARs and assess the meteorology. The results from composites obtained are generally in agreement which suggests that these ARDTs might be capturing the same meteorological phenomenon (apparently a midlatitude cyclone) at different phases of its evolution. With these findings, we refuse to accept the hypothesis that ARDTs capture different meteorological phenomena during landfall over the western coast of CONUS using different ARDTs.

ARDTs have proved to detect different flavors of ARs (Gonzales et al., 2020; Y. Zhou et al., 2022). These flavors are mostly a result of what ARDTs classify as ARs. As such we have assessed composites for landfalling ARs and their surrounding meteorological phenomena focusing on the DJF season. Four ARDTs are assessed; TECA_BARD v1, Guan & Waliser, Reid 250 and Mundhenk v3. These ARDTs capture different AR frequencies (counts) over a landfall region. From the number of counts, we are able to determine that for specific times, all four ARDTs agree on the presence of an AR in the vicinity of landfall (CTs). However, the majority of ARs detected by these ARDTs are mostly not in consensus (NCTs). We further assess unique times when only an ARDT captures an AR apart from the other ARDTs. Results show that TECA_BARD v1, Reid 250, and Mundhenk v3 ARDTs are mostly in agreement with either one of the four ARDTs, however, Guan & Waliser ARDT tends to not be in agreement as much (Table 1). The Mundhenk and Reid250 ARDTs show similar results as the Guan & Waliser ARDT with a reduction in the frequency and shape of landfalling ARs. Aside from the difference in the number of ARs and their respective times of capture, it is observed that there are different angles subtended by ARs in the ARDTs (see also Figure A1 and A2). These different spatial orientations can be observed directly from the orientations in composites. For instance, the region of steepest gradient between the high-pressure and the low-pressure systems generally determines the location of the AR. This is consistent Guirguis et al. (2019)'s findings that different surface orientations may influence the location and orientation of an AR.

In general, there is an agreement between all ARDTs on the prevailing meteorological phenomena during AR landfall, however, the magnitudes and orientations of these meteorological phenomena are statistically different. We demonstrate using composites that, there is always a prevailing surface low-pressure along the northwestern bound of the AR which tends to form a confluence region. This confluence region coupled with positive PV anomalies and a prevalent mid-tropospheric trough serves as a good source of vertical and horizontal advection for water vapor. Guirguis et al. (2023) show in their work the impact of winds at the confluence region and their importance for moisture transport during different times in the DJF season. We find that during AR events in all ARDTs, there is more warmth in the column of intense IVT as compared to the surrounding meteorology which is consistent with the findings of Mo et al. (2022). The intensity of the IVT during ARs may depend on the strength of the some variables like the surface pressure gradients and mid tropospheric PV. Our results show that during CTs, there is higher IVT and TCWV, a stronger low-pressure anomaly, higher mid-tropospheric warm temperature anomaly, and a region of strong positive to negative PV anomaly gradient along the landfall region as opposed to the NCTs. These results are consistent with findings from Lora et al. (2020) andRutz et al. (2014) which suggests that the meteorology during CTs indicates synoptic conditions that are favorable for strong IVTs. PV on the other hand shows consistency in all 4 ARDTs; there is no statistical difference in the PV captured in all 4 ARDTs. Guirguis et al. (2019) using self-organizing maps (SOMs) shows that the different orientations of the 500 hPa heights could be a result of ENSO effects contributing to AR formation and landfall. The prevalence of the anomalous geopotential heights also has been identified to be influenced by the 4 Pacific North weather regimes, namely, the Alaskan Pacific, Baja Pacific, Canadian Pacific, and Off-shore California Pacific pressure systems. For the landfall site under consideration, Guirguis et al. (2023) show in their paper that all four modes come into play when ARs are prevalent

To ascertain the significance of the difference between ARDTs, the student's t-test is computed on the differences between ARDTs. We observe that during landfall, all ARDTs are statistically different from each other. Here, our goal is not to assess the phenomenon prior to landfall, however, results from this work point in the direction that, ARDTs could have different preceding meteorology like strong or weak atmospheric or oceanic frontal systems (Liu et al., 2021), strong confluence winds resulting from different sea level pressure magnitudes (Payne & Magnusdottir, 2016), and other meteorological phenomena which could lead to them identifying different frequencies and even, types of ARs.

Assessing the difference between prevailing atmospheric conditions for ARDTs has various implications and may lead to a better understanding of what physical processes to expect during AR events. Since observations are not able to quantify specifically the morphology of ARs, ARDTs are a good proxy to identify the point where a region of IVT can be classified as an AR, however, the definition of an AR may be subject to location and period. For instance, in a changing climate, the threshold for what may be defined as an AR that leads to extreme events may change since our threshold for classifying what an extreme is may also change. This is also mentioned in the study of O'Brien et al. (2022) where they observe that the uncertainty associated with ARDTs dominates that of models. Also, in a changing climate where water vapor increases, absolute ARDTs will become more permissive because the current absolute thresholds may not be a good definition for an AR. This brings to light questions like (1) Do these ARDTs continue to detect ARs associated with similar phenomena as the climate changes? (2) Since ARs are often associated with extratropical cyclones (ETCs), how often do ARDTs actually capture ETC-induced ARs? This work shows that we are able to observe similarities in the prevailing weather patterns during an AR, however, ARDTs may have different magnitudes associated with their atmospheric composites. This suggests that for any ARDT, the effects of ARs leading to extremes will be different and as a result, capturing AR-induced extremes may be subject to which ARDT is being analyzed. In light of this, future work will involve assessing landfalling ARs in different locations globally to ascertain if the prevailing weather patterns would remain the same in all instances.

Appendix A Supplemental Plots

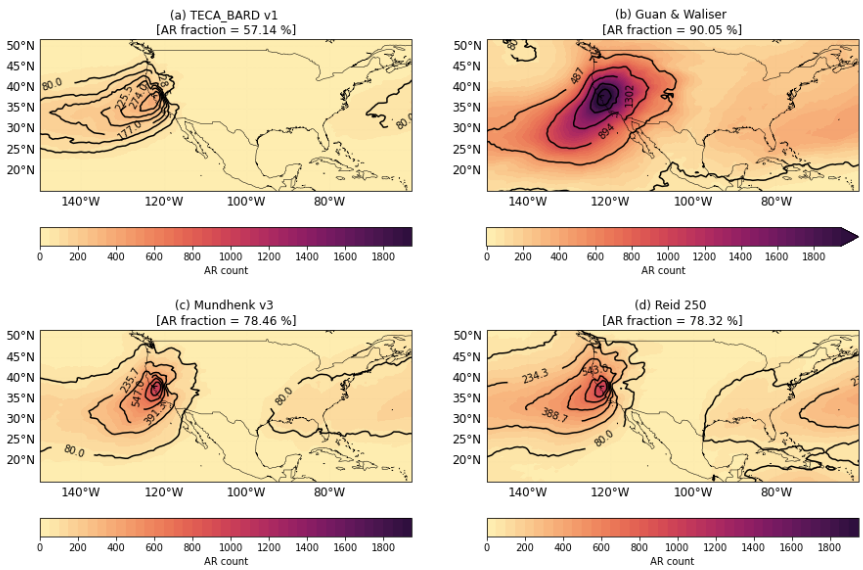

Figure A1. Non-Consensus times for land-falling ARs for all ARDTs. TECA_BARD v1 (a), Guan & Waliser (b), Mundhenk (c), Reid 250 (d). Percentages show the ratio of NCTs to the total AR frequency.

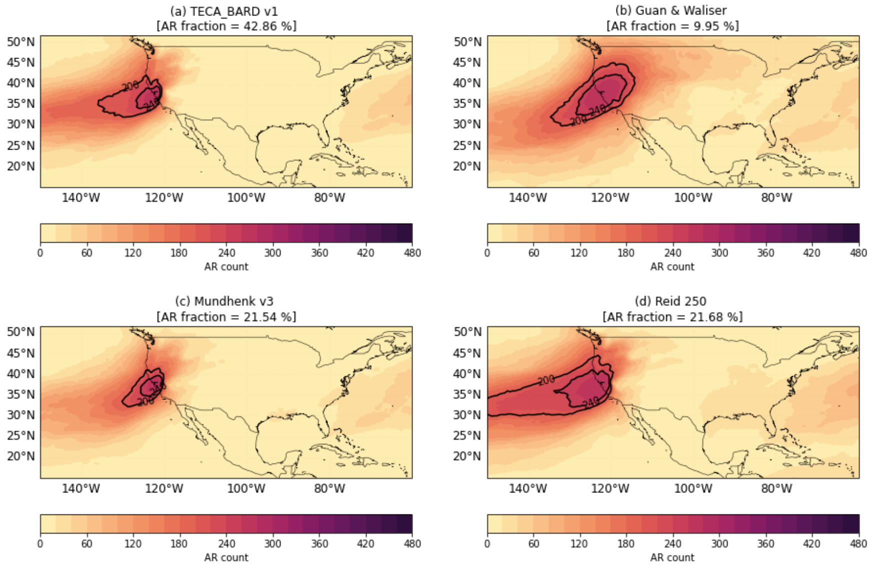

Figure A2. Consensus times for land-falling ARs for all ARDTs. TECA_BARD v1 (a), Guan & Waliser (b), Mundhenk (c), Reid 250 (d). Percentages show the ratio of CTs to the total AR frequencies.

Acknowledgments

This material is based upon work supported by the U.S. Department of Energy, Office of Science, Office of Biological and Environmental Research, Climate and Environmental Sciences Division, Regional & Global Model Analysis Program and used resources of the National Energy Research Scientific Computing Center (NERSC), also supported by the Office of Science of the U.S. Department of Energy under Contract No. DE-AC02-05CH11231. This research was supported in part by Lilly Endowment, Inc., through its support for the Indiana University Pervasive Technology Institute.

References

Bao, J., Michelson, S., Neiman, P., Ralph, F., & Wilczak, J. (2006). Interpretation of enhanced integrated water vapor bands associated with extratropical cyclones: Their formation and connection to tropical moisture. *Monthly weather review*, *134*(4), 1063–1080.

Barth, N. A., Villarini, G., Nayak, M. A., & White, K. (2017). Mixed populations and annual flood frequency estimates in the western united states: The role of atmospheric rivers. *Water Resources Research*, *53*(1), 257–269.

Blamey, R., Ramos, A., Trigo, R., Tomé, R., & Reason, C. (2018). The influence of atmospheric rivers over the south atlantic on winter rainfall in south africa. *Journal of Hydrometeorology*, *19*(1), 127–142.

Bluestein, H. B. (1992). *Synoptic-dynamic meteorology in midlatitudes: Observations and theory of weather systems* (Vol. 2). Taylor & Francis.

Dettinger, M. (2011). Climate change, atmospheric rivers, and floods in california–a multimodel analysis of storm frequency and magnitude changes 1. *JAWRA*

Journal of the American Water Resources Association, *47*(3), 514–523.
Dettinger, M. D. (2013). Atmospheric rivers as drought busters on the us west coast. *Journal of Hydrometeorology*, *14*(6), 1721–1732.
Dhana Laskhmi, D., & Satyanarayana, A. (2020). Climatology of landfalling atmospheric rivers and associated heavy precipitation over the indian coastal regions. *International Journal of Climatology*, *40*(13), 5616–5633.
Doiteau, B., Dournaux, M., Montoux, N., & Baray, J.-L. (2021). Atmospheric rivers and associated precipitation over france and western europe: 1980–2020 climatology and case study. *Atmosphere*, *12*(8), 1075.
Gelaro, R., McCarty, W., Suárez, M. J., Todling, R., Molod, A., Takacs, L., ... others (2017). The modern-era retrospective analysis for research and applications, version 2 (merra-2). *Journal of climate*, *30*(14), 5419–5454.
Gershunov, A., Shulgina, T., Clemesha, R. E., Guirguis, K., Pierce, D. W., Dettinger, M. D., ... others (2019). Precipitation regime change in western north america: the role of atmospheric rivers. *Scientific reports*, *9*(1), 9944.
Gershunov, A., Shulgina, T., Ralph, F. M., Lavers, D. A., & Rutz, J. J. (2017). Assessing the climate-scale variability of atmospheric rivers affecting western north america. *Geophysical Research Letters*, *44*(15), 7900–7908.
Goldenson, N., Leung, L., Bitz, C. M., & Blanchard-Wrigglesworth, E. (2018). Influence of atmospheric rivers on mountain snowpack in the western united states. *Journal of Climate*, *31*(24), 9921–9940.
Gonzales, K. R., Swain, D. L., Barnes, E. A., & Diffenbaugh, N. S. (2020). Moisture-versus wind-dominated flavors of atmospheric rivers. *Geophysical Research Letters*, *47*(23), e2020GL090042.
Guan, B., Molotch, N. P., Waliser, D. E., Fetzer, E. J., & Neiman, P. J. (2010). Extreme snowfall events linked to atmospheric rivers and surface air temperature via satellite measurements. *Geophysical Research Letters*, *37*(20).
Guan, B., & Waliser, D. E. (2015). Detection of atmospheric rivers: Evaluation and application of an algorithm for global studies. *Journal of Geophysical Research: Atmospheres*, *120*(24), 12514–12535.
Guirguis, K., Gershunov, A., Hatchett, B., Shulgina, T., DeFlorio, M. J., Subramanian, A. C., ... others (2023). Winter wet–dry weather patterns driving atmospheric rivers and santa ana winds provide evidence for increasing wildfire hazard in california. *Climate Dynamics*, *60*(5-6), 1729–1749.
Guirguis, K., Gershunov, A., Shulgina, T., Clemesha, R. E., & Ralph, F. M. (2019). Atmospheric rivers impacting northern california and their modulation by a variable climate. *Climate Dynamics*, *52*, 6569–6583.
Hagos, S., Leung, L. R., Yang, Q., Zhao, C., & Lu, J. (2015). Resolution and dynamical core dependence of atmospheric river frequency in global model simulations. *Journal of Climate*, *28*(7), 2764–2776.
Hersbach, H., Bell, B., Berrisford, P., Hirahara, S., Horányi, A., Muñoz-Sabater, J., ... others (2020). The era5 global reanalysis. *Quarterly Journal of the Royal Meteorological Society*, *146*(730), 1999–2049.
Inda-Díaz, H. A., O'Brien, T. A., Zhou, Y., & Collins, W. D. (2021). Constraining and characterizing the size of atmospheric rivers: A perspective independent from the detection algorithm. *Journal of Geophysical Research: Atmospheres*, *126*(16), e2020JD033746.
Jankov, I., Bao, J.-W., Neiman, P. J., Schultz, P. J., Yuan, H., & White, A. B. (2009). Evaluation and comparison of microphysical algorithms in arw-wrf model simulations of atmospheric river events affecting the california coast. *Journal of Hydrometeorology*, *10*(4), 847–870.
Junker, N. W., Grumm, R. H., Hart, R., Bosart, L. F., Bell, K. M., & Pereira, F. J. (2008). Use of normalized anomaly fields to anticipate extreme rainfall in the mountains of northern california. *Weather and forecasting*, *23*(3), 336–356.
Kashinath, K., Mudigonda, M., Kim, S., Kapp-Schwoerer, L., Graubner, A., Karais-

mailoglu, E., ... others (2021). Climatenet: an expert-labeled open dataset and deep learning architecture for enabling high-precision analyses of extreme weather. *Geoscientific Model Development*, *14*(1), 107–124.

Kim, H.-M., Zhou, Y., & Alexander, M. A. (2019). Changes in atmospheric rivers and moisture transport over the northeast pacific and western north america in response to enso diversity. *Climate Dynamics*, *52*(12), 7375–7388.

Kunkel, K. E., & Champion, S. M. (2019). An assessment of rainfall from hurricanes harvey and florence relative to other extremely wet storms in the united states. *Geophysical Research Letters*, *46*(22), 13500–13506.

Lamjiri, M. A., Dettinger, M. D., Ralph, F. M., & Guan, B. (2017). Hourly storm characteristics along the us west coast: Role of atmospheric rivers in extreme precipitation. *Geophysical Research Letters*, *44*(13), 7020–7028.

Lavers, D. A., & Villarini, G. (2015). The contribution of atmospheric rivers to precipitation in europe and the united states. *Journal of Hydrology*, *522*, 382–390.

Lavers, D. A., Villarini, G., Allan, R. P., Wood, E. F., & Wade, A. J. (2012). The detection of atmospheric rivers in atmospheric reanalyses and their links to british winter floods and the large-scale climatic circulation. *Journal of Geophysical Research: Atmospheres*, *117*(D20).

Leung, L. R., & Qian, Y. (2009). Atmospheric rivers induced heavy precipitation and flooding in the western us simulated by the wrf regional climate model. *Geophysical research letters*, *36*(3).

Liu, X., Ma, X., Chang, P., Jia, Y., Fu, D., Xu, G., ... Patricola, C. M. (2021). Ocean fronts and eddies force atmospheric rivers and heavy precipitation in western north america. *Nature communications*, *12*(1), 1268.

Lora, J. M., Mitchell, J. L., Risi, C., & Tripati, A. E. (2017). North pacific atmospheric rivers and their influence on western north america at the last glacial maximum. *Geophysical Research Letters*, *44*(2), 1051–1059.

Lora, J. M., Shields, C., & Rutz, J. (2020). Consensus and disagreement in atmospheric river detection: Artmip global catalogues. *Geophysical Research Letters*, *47*(20), e2020GL089302.

Mahoney, K., Jackson, D. L., Neiman, P., Hughes, M., Darby, L., Wick, G., ... Cifelli, R. (2016). Understanding the role of atmospheric rivers in heavy precipitation in the southeast united states. *Monthly Weather Review*, *144*(4), 1617–1632.

McIntyre, M. E. (2003). Potential vorticity. *Encyclopedia of atmospheric sciences*, *2*, 685–694.

Mo, R., Lin, H., & Vitart, F. (2022). An anomalous warm-season trans-pacific atmospheric river linked to the 2021 western north america heatwave. *Communications Earth & Environment*, *3*(1), 1–12.

Mundhenk, B. D., Barnes, E. A., & Maloney, E. D. (2016). All-season climatology and variability of atmospheric river frequencies over the north pacific. *Journal of Climate*, *29*(13), 4885–4903.

Nayak, M. A., Villarini, G., & Lavers, D. A. (2014). On the skill of numerical weather prediction models to forecast atmospheric rivers over the central united states. *Geophysical Research Letters*, *41*(12), 4354–4362.

Neiman, P. J., Ralph, F. M., Wick, G. A., Lundquist, J. D., & Dettinger, M. D. (2008). Meteorological characteristics and overland precipitation impacts of atmospheric rivers affecting the west coast of north america based on eight years of ssm/i satellite observations. *Journal of Hydrometeorology*, *9*(1), 22–47.

O'Brien, T. A., Risser, M. D., Loring, B., Elbashandy, A. A., Krishnan, H., Johnson, J., ... others (2020). Detection of atmospheric rivers with inline uncertainty quantification: Teca-bard v1. 0.1. *Geoscientific Model Development*, *13*(12), 6131–6148.

O'Brien, T. A., Wehner, M. F., Payne, A. E., Shields, C. A., Rutz, J. J., Leung,

L.-R., … others (2022). Increases in future ar count and size: Overview of the artmip tier 2 cmip5/6 experiment. *Journal of Geophysical Research: Atmospheres*, *127*(6), e2021JD036013.
Pan, M., & Lu, M. (2019). A novel atmospheric river identification algorithm. *Water Resources Research*, *55*(7), 6069–6087.
Payne, A. E., & Magnusdottir, G. (2014). Dynamics of landfalling atmospheric rivers over the north pacific in 30 years of merra reanalysis. *Journal of Climate*, *27*(18), 7133–7150.
Payne, A. E., & Magnusdottir, G. (2015). An evaluation of atmospheric rivers over the north pacific in cmip5 and their response to warming under rcp 8.5. *Journal of Geophysical Research: Atmospheres*, *120*(21), 11–173.
Payne, A. E., & Magnusdottir, G. (2016). Persistent landfalling atmospheric rivers over the west coast of north america. *Journal of Geophysical Research: Atmospheres*, *121*(22), 13–287.
Ralph, F., Coleman, T., Neiman, P., Zamora, R., & Dettinger, M. (2013). Observed impacts of duration and seasonality of atmospheric-river landfalls on soil moisture and runoff in coastal northern california. *Journal of Hydrometeorology*, *14*(2), 443–459.
Ralph, F. M., & Dettinger, M. D. (2011). Storms, floods, and the science of atmospheric rivers. *Eos, Transactions American Geophysical Union*, *92*(32), 265–266.
Ralph, F. M., Neiman, P. J., & Wick, G. A. (2004). Satellite and caljet aircraft observations of atmospheric rivers over the eastern north pacific ocean during the winter of 1997/98. *Monthly Weather Review*, *132*(7), 1721–1745.
Ralph, F. M., Rutz, J. J., Cordeira, J. M., Dettinger, M., Anderson, M., Reynolds, D., … Smallcomb, C. (2019). A scale to characterize the strength and impacts of atmospheric rivers. *Bulletin of the American Meteorological Society*, *100*(2), 269–289.
Reid, K. J., King, A. D., Lane, T. P., & Short, E. (2020). The sensitivity of atmospheric river identification to integrated water vapor transport threshold, resolution, and regridding method. *Journal of Geophysical Research: Atmospheres*, *125*(20), e2020JD032897.
Rutz, J. J., Shields, C. A., Lora, J. M., Payne, A. E., Guan, B., Ullrich, P., … Viale, M. (2019a). The atmospheric river tracking method intercomparison project (artmip): Quantifying uncertainties in atmospheric river climatology. *Journal of Geophysical Research: Atmospheres*, *124*(24), 13777-13802. Retrieved from `https://agupubs.onlinelibrary.wiley.com/doi/abs/10.1029/2019JD030936` doi: https://doi.org/10.1029/2019JD030936
Rutz, J. J., Shields, C. A., Lora, J. M., Payne, A. E., Guan, B., Ullrich, P., … others (2019b). The atmospheric river tracking method intercomparison project (artmip): quantifying uncertainties in atmospheric river climatology. *Journal of Geophysical Research: Atmospheres*, *124*(24), 13777–13802.
Rutz, J. J., & Steenburgh, W. J. (2012). Quantifying the role of atmospheric rivers in the interior western united states. *Atmospheric Science Letters*, *13*(4), 257–261.
Rutz, J. J., Steenburgh, W. J., & Ralph, F. M. (2014). Climatological characteristics of atmospheric rivers and their inland penetration over the western united states. *Monthly Weather Review*, *142*(2), 905–921.
Ryoo, J.-M., Kaspi, Y., Waugh, D. W., Kiladis, G. N., Waliser, D. E., Fetzer, E. J., & Kim, J. (2013). Impact of rossby wave breaking on us west coast winter precipitation during enso events. *Journal of Climate*, *26*(17), 6360–6382.
Shields, C. (2019). *Artmip tier 1 catalogues. ucar/ncar - climate and global dynamics laboratory.* https://doi.org/10.5065/D6R78D1M. (Accessed 06 February 2023)
Shields, C. A., Payne, A. E., Shearer, E. J., Wehner, M. F., O'Brien, T. A., Rutz, J. J., … others (2023). Future atmospheric rivers and impacts on precipita-

tion: Overview of the artmip tier 2 high-resolution global warming experiment. *Geophysical Research Letters*, *50*(6), e2022GL102091.
Shields, C. A., Rutz, J. J., Leung, L.-Y., Ralph, F. M., Wehner, M., Kawzenuk, B., ... others (2018). Atmospheric river tracking method intercomparison project (artmip): project goals and experimental design. *Geoscientific Model Development*, *11*(6), 2455–2474.
Turner, J., Lu, H., King, J. C., Carpentier, S., Lazzara, M., Phillips, T., & Wille, J. (2022). An extreme high temperature event in coastal east antarctica associated with an atmospheric river and record summer downslope winds. *Geophysical Research Letters*, *49*(4), e2021GL097108.
Williams, A. P., Cook, E. R., Smerdon, J. E., Cook, B. I., Abatzoglou, J. T., Bolles, K., ... Livneh, B. (2020). Large contribution from anthropogenic warming to an emerging north american megadrought. *Science*, *368*(6488), 314–318.
Xiong, Y., & Ren, X. (2021). Influences of atmospheric rivers on north pacific winter precipitation: Climatology and dependence on enso condition. *Journal of Climate*, *34*(1), 277–292.
Zhang, J., Jia, Y., Ji, R., & Wu, Y. (2021). Decadal variation of atmospheric rivers in relation to north atlantic tripole sst mode. *Atmosphere*, *12*(10), 1252.
Zhou, T.-J., & Yu, R.-C. (2005). Atmospheric water vapor transport associated with typical anomalous summer rainfall patterns in china. *Journal of Geophysical Research: Atmospheres*, *110*(D8).
Zhou, Y., O'Brien, T. A., Collins, W. D., Shields, C. A., Loring, B., & Elbashandy, A. A. (2022). Characteristics and variability of winter northern pacific atmospheric river flavors. *Journal of Geophysical Research: Atmospheres*, *127*(23), e2022JD037105.
Zhu, Y., & Newell, R. E. (1998). A proposed algorithm for moisture fluxes from atmospheric rivers. *Monthly weather review*, *126*(3), 725–735.